Electronic Supplementary Material (ESI) for Organic & Biomolecular Chemistry

Supplementary material

Chemoenzymatic synthesis, structural study and biological activity of novel indolizidine and quinolizidine iminocyclitols

Livia Gómez[a], Xavier Garrabou[a], Jesús Joglar[a], Jordi Bujons[a], Teodor Parella[b], Cristina Vilaplana[c], Pere Joan Cardona[c], Pere Clapés[a]*

[a]Dept Biological Chemistry and Molecular Modeling. Instituto de Química Avanzada de Cataluña, IQAC-CSIC. Jordi Girona 18-26, 08034 Barcelona, Spain.

[b]Servei de Ressonància Magnètica Nuclear, Departament de Química. Universitat Autònoma de Barcelona, Bellaterra, Spain.

[c]Unitat de Tuberculosi Experimental. Fundació Institut d'Investigació en Ciències de la Salut Germans Trias i Pujol. Edifici Laboratoris de Recerca. Crtra. de Can Ruti, Camí de les Escoles, s/n, 08916, Badalona (Spain)

Enzymatic inhibition assays against commercial glycosidases

Commercial glycosidase solutions were prepared with the appropriate buffer and incubated in 96-well plates at 37ºC without (control) or with inhibitor (1.6 mM to 4.2 nM) during 3 min for α-D-glucosidase, β-D-glucosidase, α-D-mannosidase, α-L-rhamnosidase, α-L-fucosidase and 5 min for β-D-galactosidase. After addition of the corresponding substrate solution, incubations were prolonged during different time periods: 10 min for α-D-glucosidase, 3 min for β-D-glucosidase, 6 min for α-D-mannosidase, 5 min for α-L-rhamnosidase, 7 min for α-L-fucosidase and 16 min for β-D-galactosidase and stopped by addition of Tris solution (50 μL, 1 M) or glycine buffer (180 μL, 100 mM, pH 10), depending on the enzymatic inhibition assay. The amount of *p*-nitrophenol formed was determined at 405 nm with UV/VIS Spectramax Plus (Molecular Devices Corporation) spectrophotometer. α-D-Glucosidase from rice activity was determined with *p*-nitrophenyl-α-D-glucopyranoside (1 mM) in sodium acetate buffer (50 mM, pH 5.0). β-D-Glucosidase activity was determined with *p*-nitrophenyl-β-D-glucopyranoside (1 mM) in sodium acetate buffer (100 mM, pH 5.0). β-D-Galactosidase activity was determined with *p*-nitrophenyl-β-D-galactopyranoside (1 mM) in sodium phosphate buffer (100 mM, 0.1 mM $MgCl_2$, pH 7.2). α-D-Mannosidase activity was determined with *p*-nitrophenyl-α-D-mannopyranoside (1 mM) in sodium acetate buffer (50 mM, pH 5.0). α-L-Rhamnosidase activity was determined with *p*-nitrophenyl-α-D-rhamnopyranoside (1 mM) in sodium acetate buffer (50 mM, pH 5.0). α-L-Fucosidase activity was determined with *p*-nitrophenyl-α-D-fucopyranoside (0.15 mM) in sodium acetate buffer (50 mM, pH 5.0). The commercial glycosidase solutions were prepared as follows: α-D-glucosidase $(NH_4)_2SO_4$ suspension (100 μL) in buffer (5 mL); β-D-glucosidase: (0.1 mg mL^{-1} buffer), β-D-galactosidase from *Aspergillus oryzae* (0.5 mg mL^{-1} buffer), α-L-rhamnosidase (naringinase) (0.3 mg mL^{-1} buffer); α-D-mannosidase $(NH_4)_2SO_4$ suspension (25 μL) in buffer (10 mL); β-D-galactosidase from bovine liver (0.1 mg mL^{-1} buffer), and α-L-fucosidase $(NH_4)_2SO_4$ suspension (33 μL) in buffer (10 mL).

Kinetics of inhibition. The nature of the inhibition against enzymes and the K_i values were determined from the Lineweaver-Burk plots.

Inhibition assays against rat intestinal disaccharidases. *Animals*. Adult male Sprague-Dawley rats weighing 200 g (n=2) (Harlan Ibèrica, Barcelona, Spain) were housed in cages (n=2/cage) under controlled conditions of a 12 hours light:dark cycle, with a temperature of 22 ± 3 ºC and a relative humidity of 40-70%. Rats were fed on a standard diet (Panlab A04, Panlab, Barcelona, Spain) and water *ad libitum*. Handling and sacrificing of the animals were in full accordance with the European Community guidelines for the care and management of laboratory animals and the pertinent permission was obtained from the CSIC Subcommittee of Bioethical issues (permit number: CTQ2009-07359). Rats were fasted overnight and then anesthetized by intramuscular injection of ketamine chlorhydrate (0.1 % v/weight of rat, (90 mg/kg body wt ip) and xylacine (0.01 % v/weight of rat, 10 mg/kg body wt ip).

Preparation of gut mucosal suspension. Small intestine was removed, and carefully divided into duodenum, jejunum and ileum. The jejunum was washed with ice-cold isotonic saline, opened lengthwise and the mucosa scraped off with a microscope slide. The jejunum mucosa was stored at –80ºC. The samples were diluted with ice-cold isotonic saline (50 mg mucosa mL^{-1}) and homogenized with a 2 mL glass homogenizer (T10 basic Ultra-Turrax , IKA, Staufen, Germany).

Assay of disaccharidase activity. Disaccharidase activities, i.e. sucrase, lactase, maltase and trehalase, in the homogenized jejunum mucosa were determined by the method of Dahlqvist.[1] Enzyme activity (µmol of substrate hydrolyzed per hour) were normalized to protein content evaluated by the method of Bradford.[2] The disaccharide substrates, sucrose, lactose, maltose and trehalose, were purchased at the highest purity available (Sigma Chemical Co.) Substrates and inhibitors were prepared in distilled water. The concentrations used in the assay were 0.02 M for disaccharides, and a range from 2 mM down for inhibitors. The homogenized mucosa was diluted four times for the sucrose and trehalase assays; one time for the lactase assay and 25 times for the maltase activity and protein determination assays. Inhibitors and suitably diluted homogenized mucosa were pre incubated for 30 minutes at 37 ºC. Then, the reaction was carried out by the addition of the substrate in phosphate buffer pH 6.8. Substrate, inhibitor and homogenized mucosa were incubated together for 30 min at 37 ºC and agitation (250 r.p.m.). The reaction was terminated by the addition of Tris-glucose oxidase-peroxidase reagent: Tris 0.5 M; 4-hydroxybenzoic acid 10 mM; 4-aminoantipyrine 0.4 mM; glucose oxidase 1480 U L^{-1}, peroxidase 250 U L^{-1}, pH 7.3. Glucose is transformed in gluconic

acid and hydrogen peroxide by glucose oxidase. Peroxidase catalyses the combination of hydrogen peroxide with 4-aminoantipiryne generating a stable and colored compound. After a further incubation of 2 hours this product was measured spectrophotometrically at 505 nm.

Figure S1. Observed NMR spectra of **3a**: a) ^{1}H, b) 2D ^{1}H-^{1}H COSY and 2D multiplicity-edited HSQC and c) selective 1D NOESY spectra.

a)

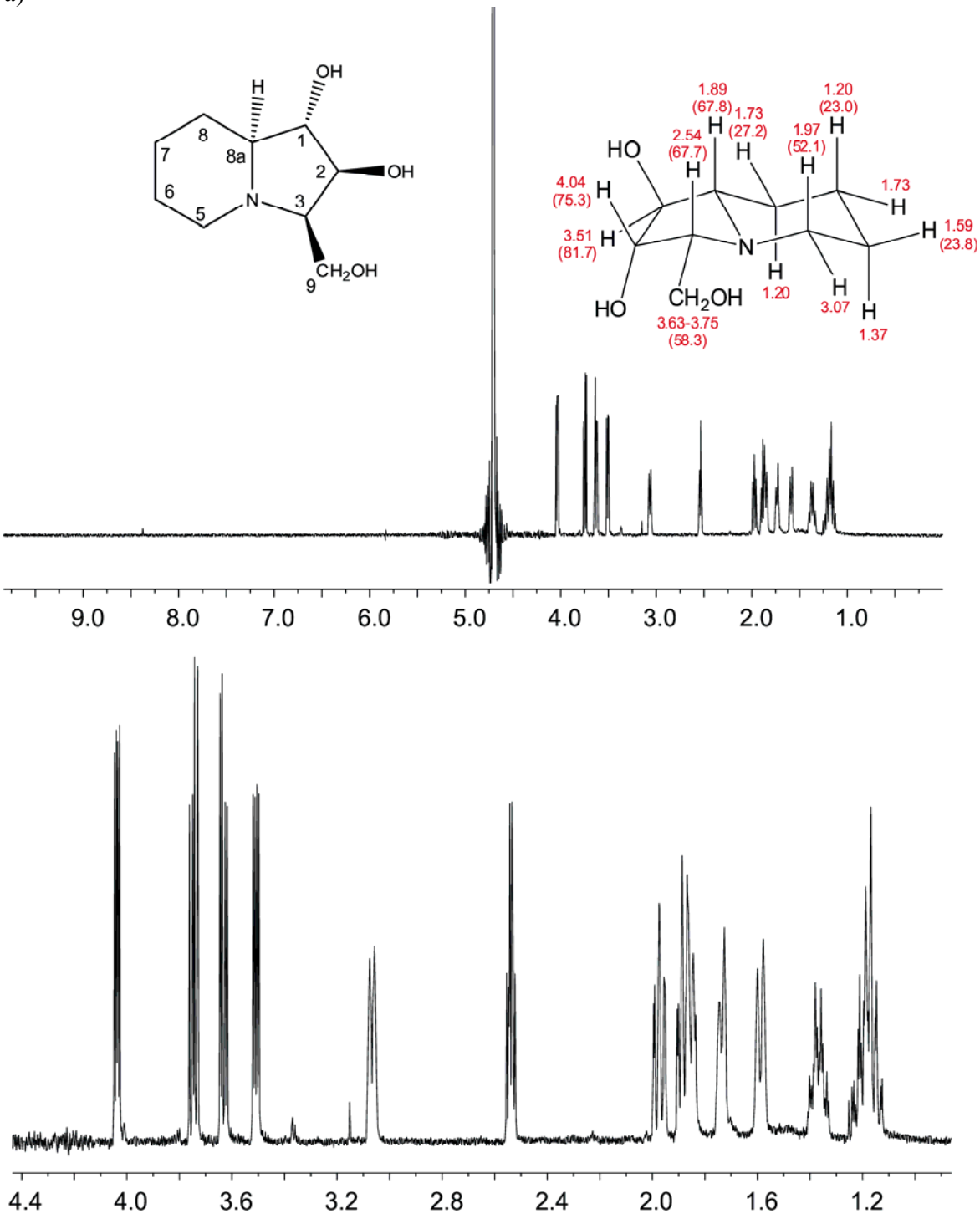

b)

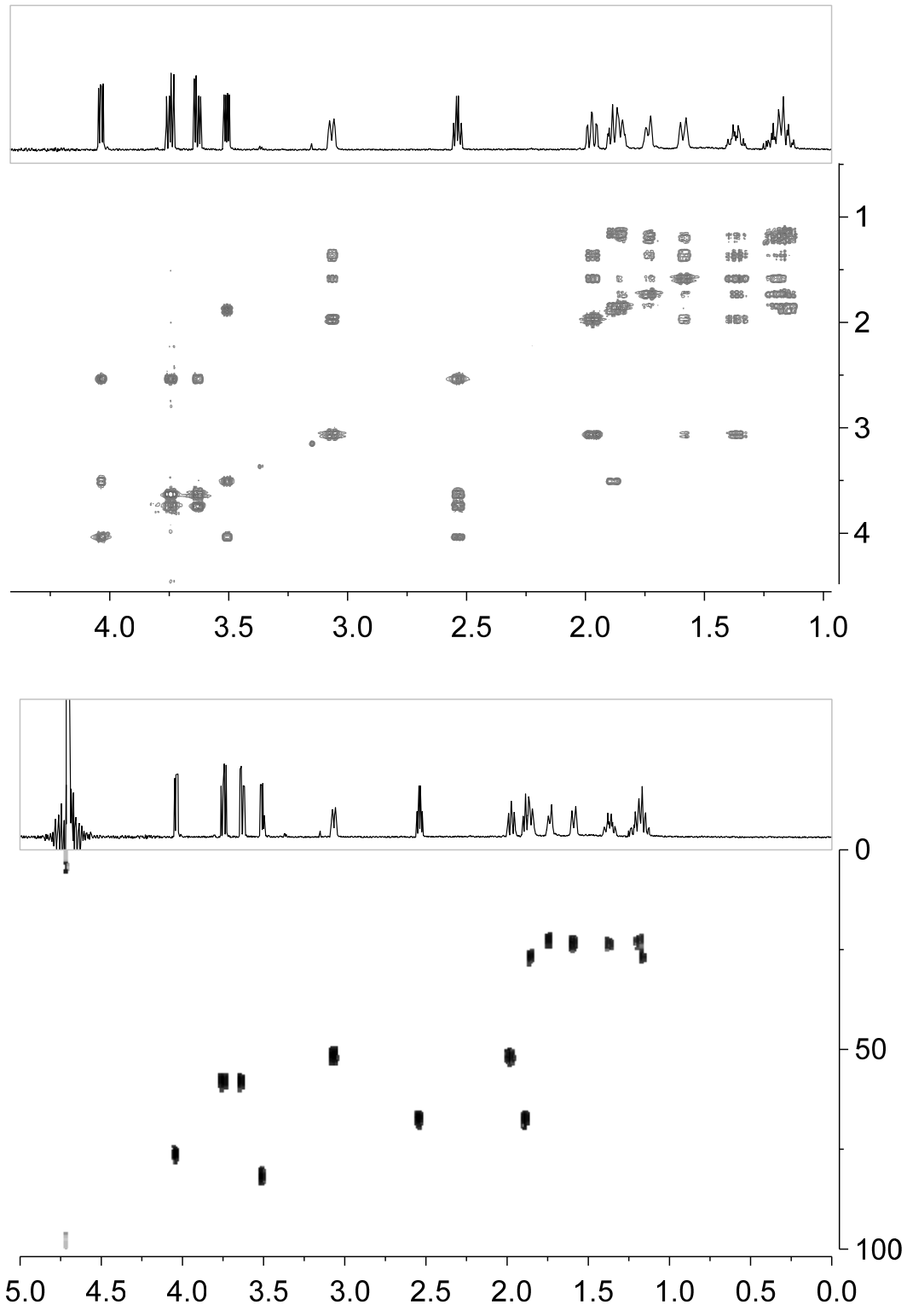

c)

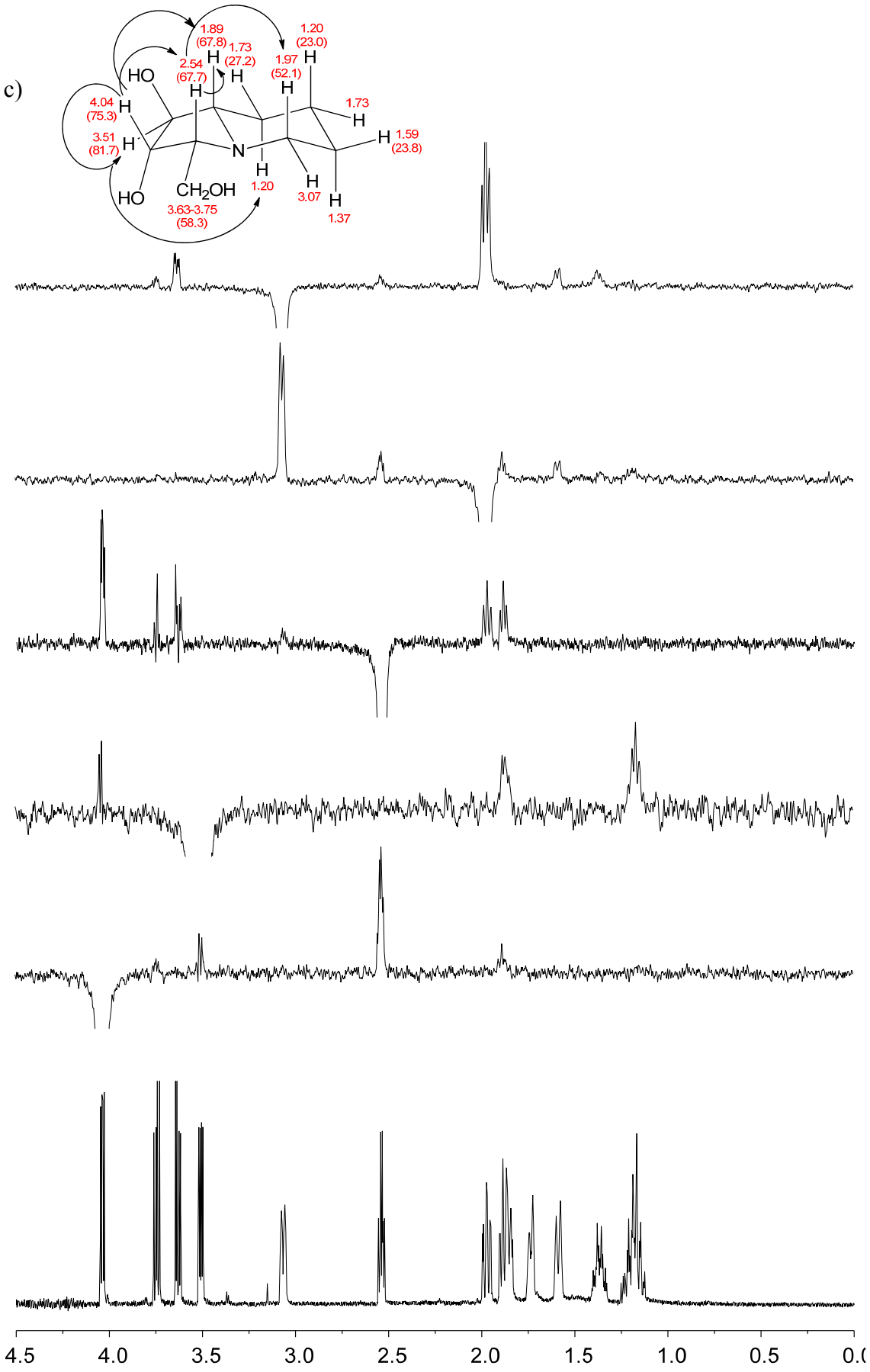

Figure S2. Observed NMR spectra of **3b**: a) ^{1}H b) 2D ^{1}H-^{1}H COSY and 2D multiplicity-edited HSQC, c) NOESY and d) selective 1D NOESY spectra.

a)

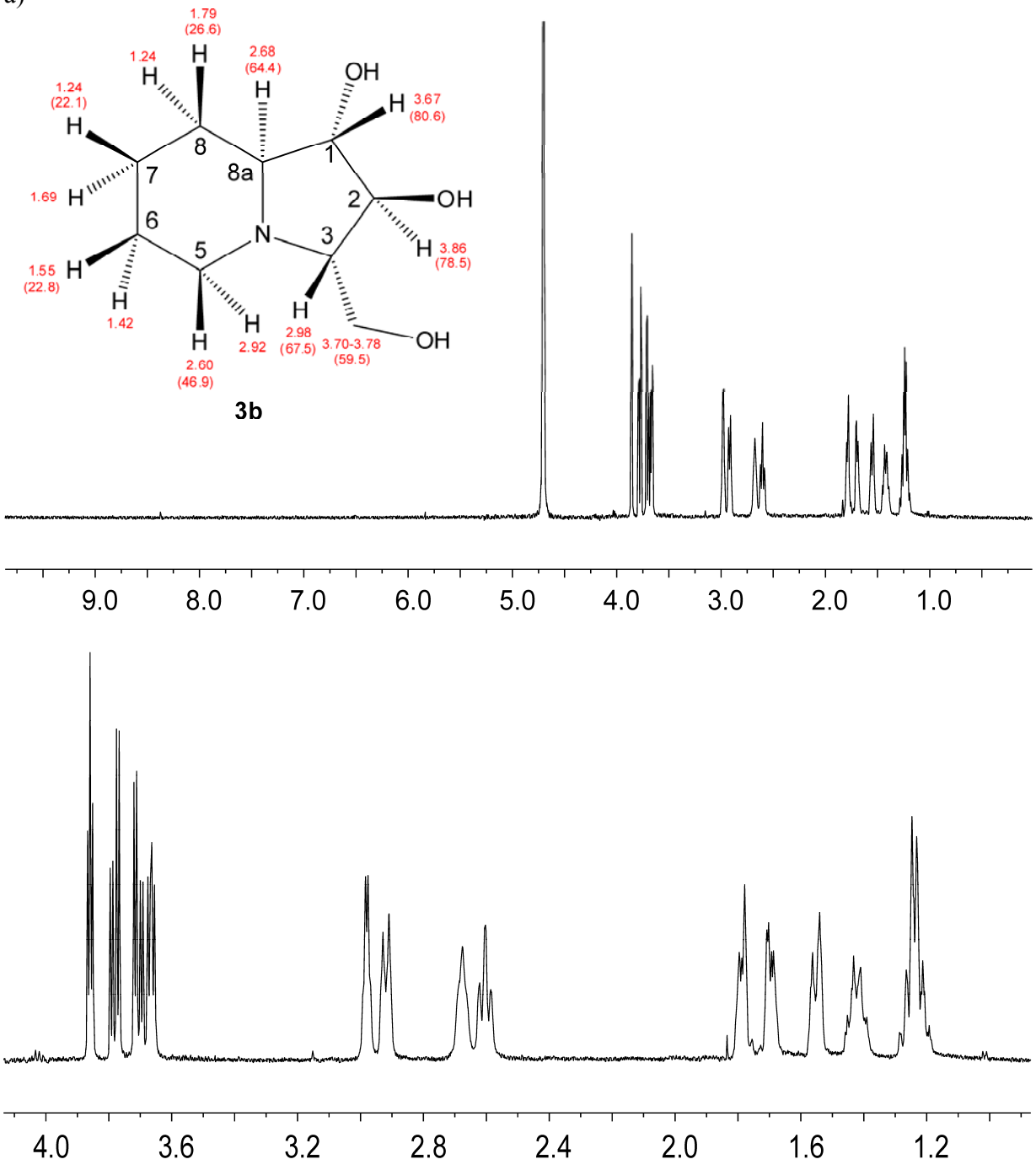

b)

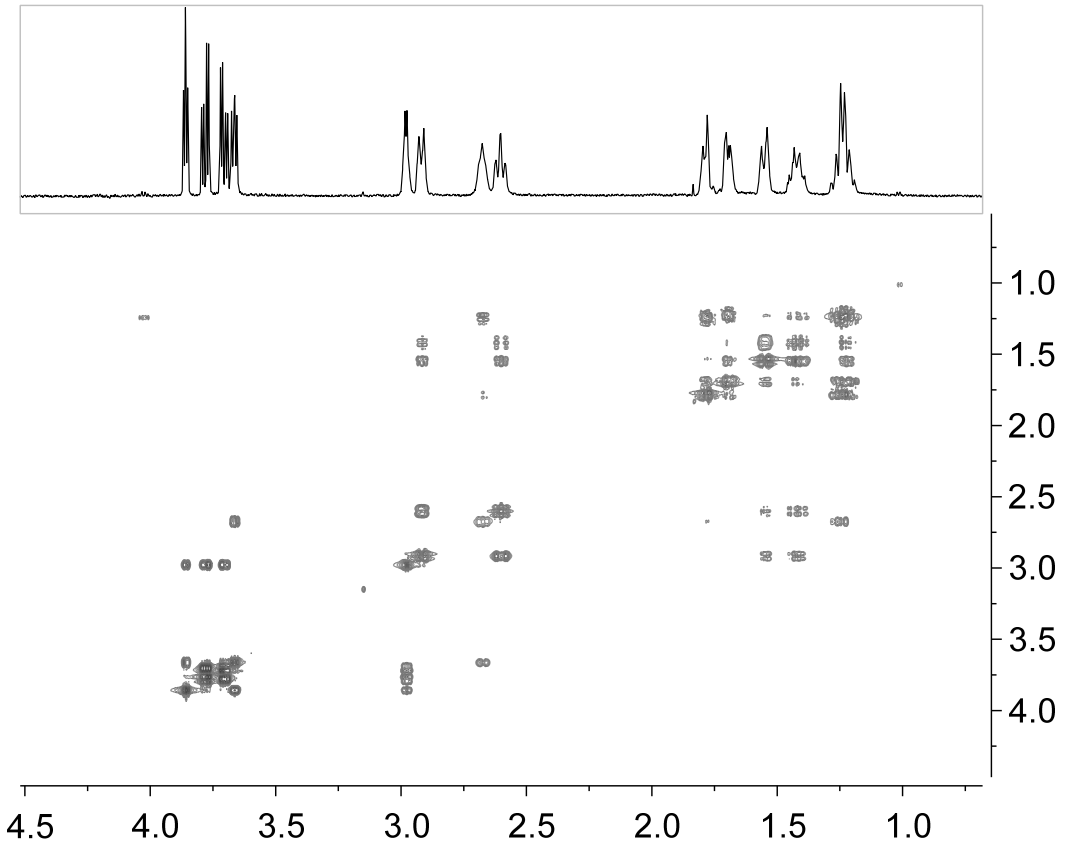

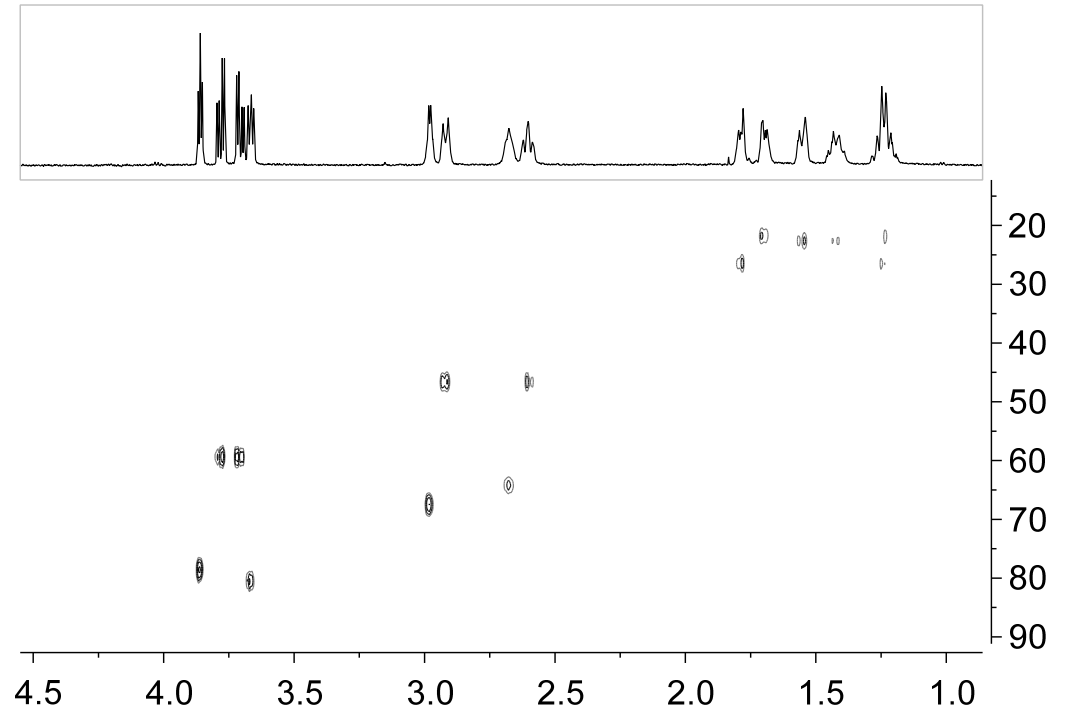

c)

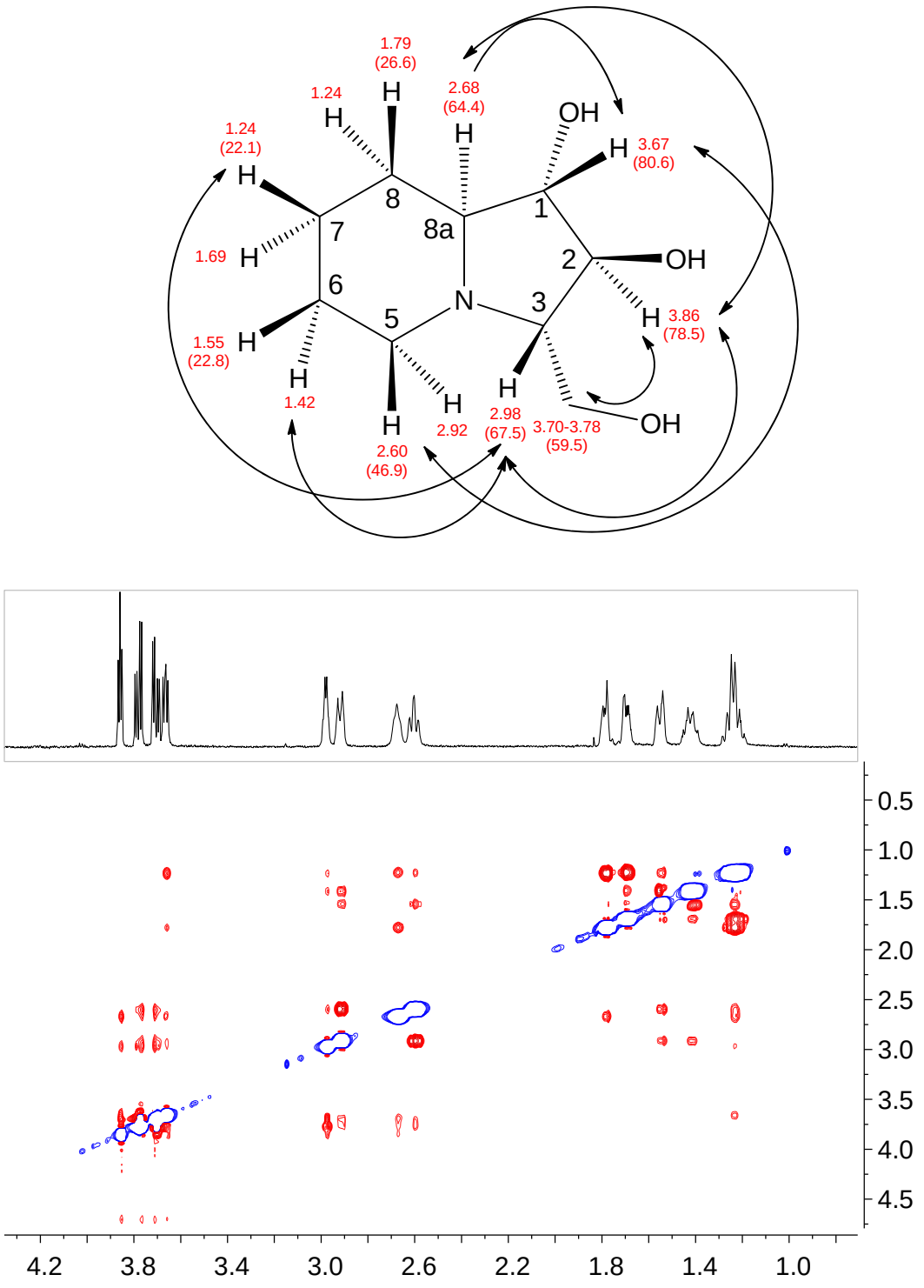

d)

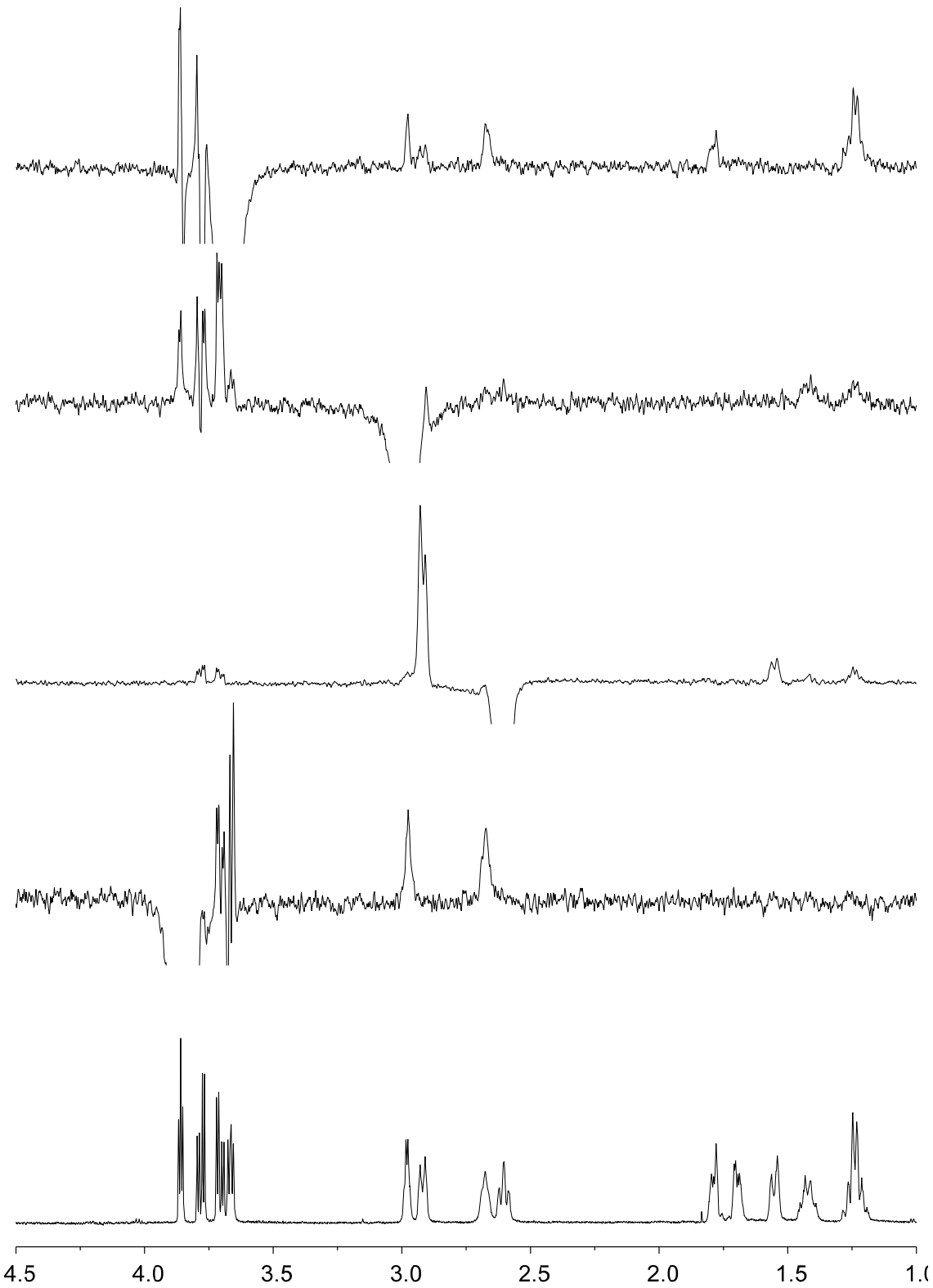

Figure S3. Observed NMR spectra of **3c**: a) ^{1}H b) 2D ^{1}H-^{1}H COSY and 2D multiplicity-edited HSQC and c) 2D NOESY spectra.

a)

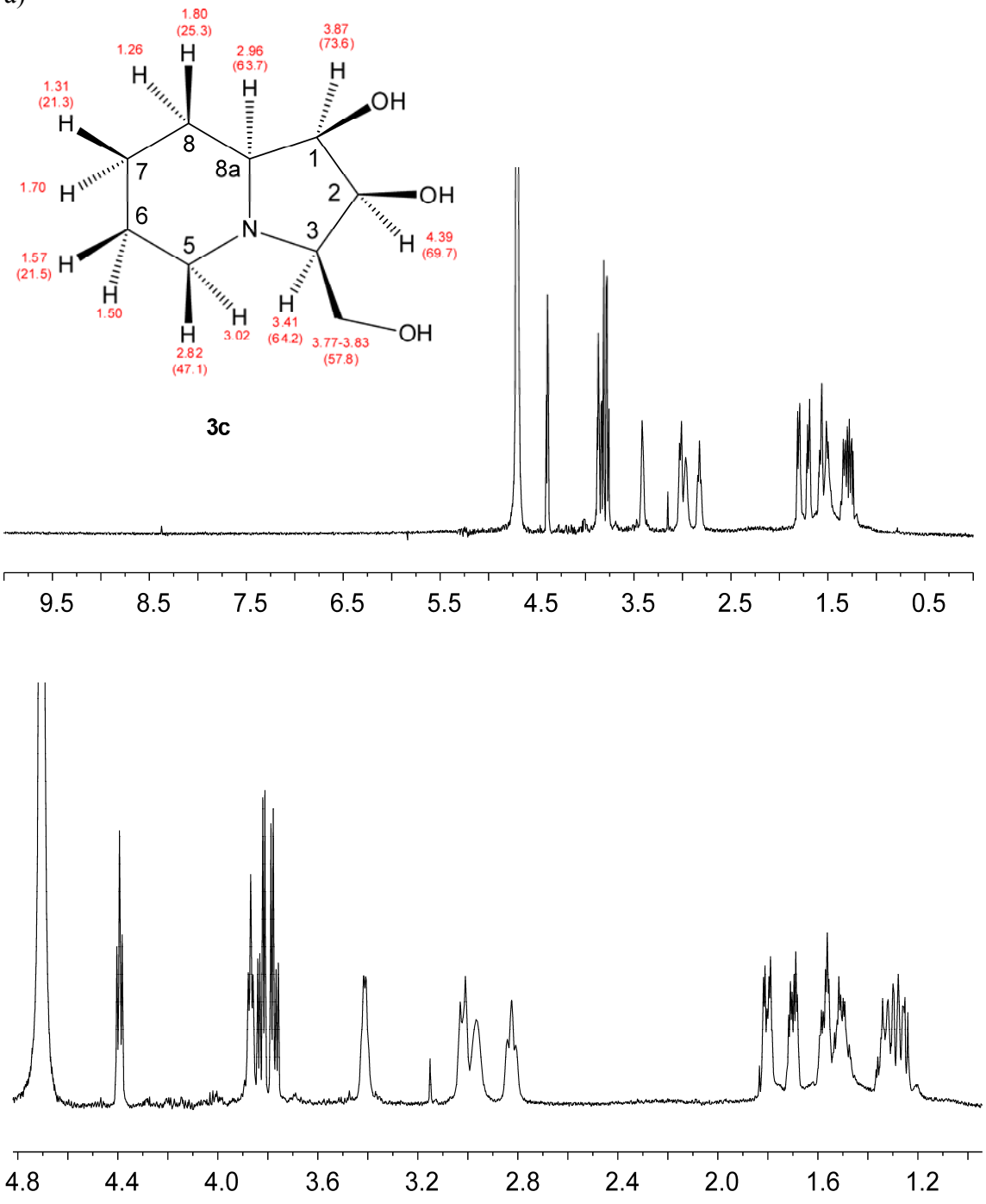

b)

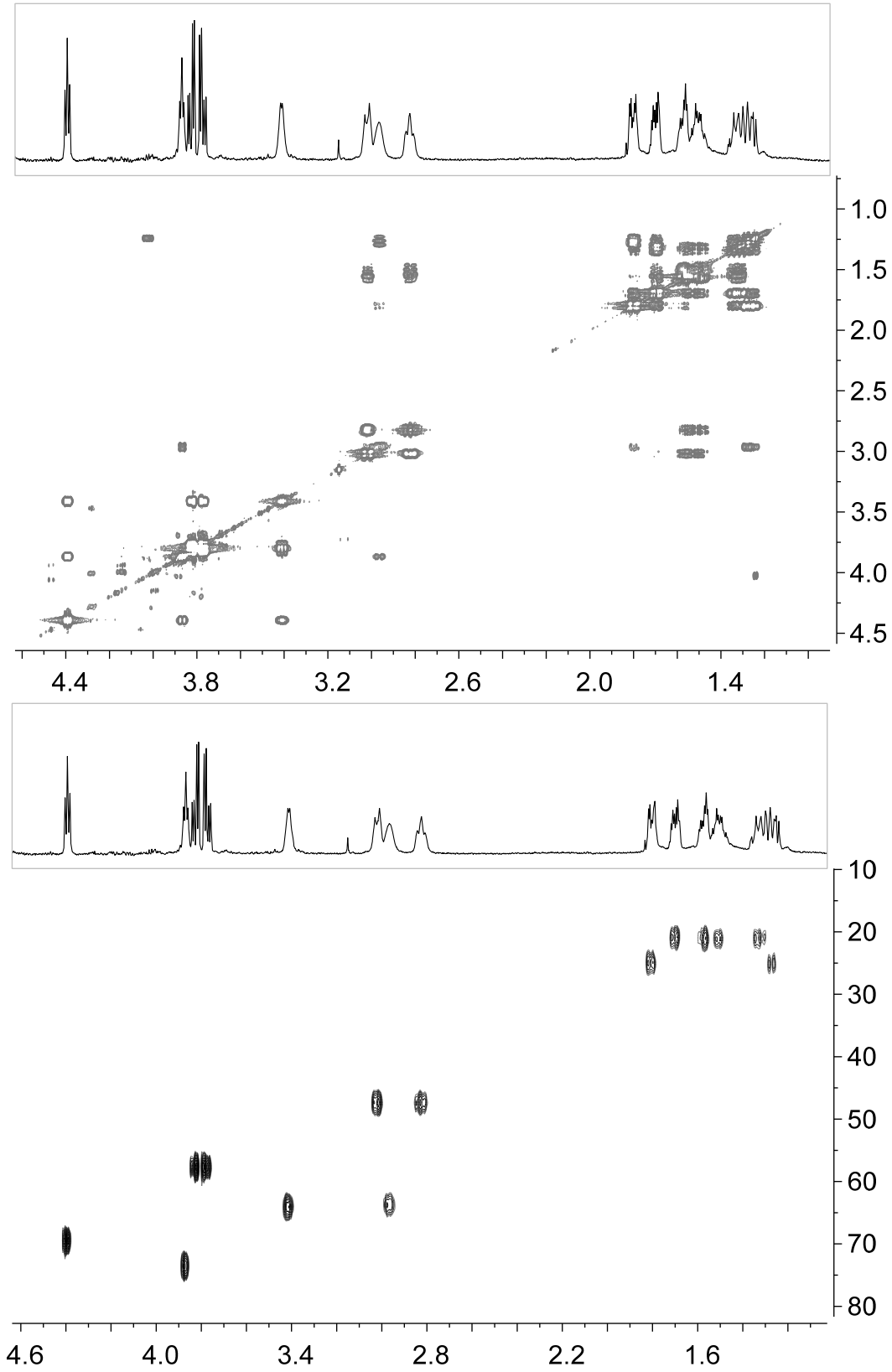

c)

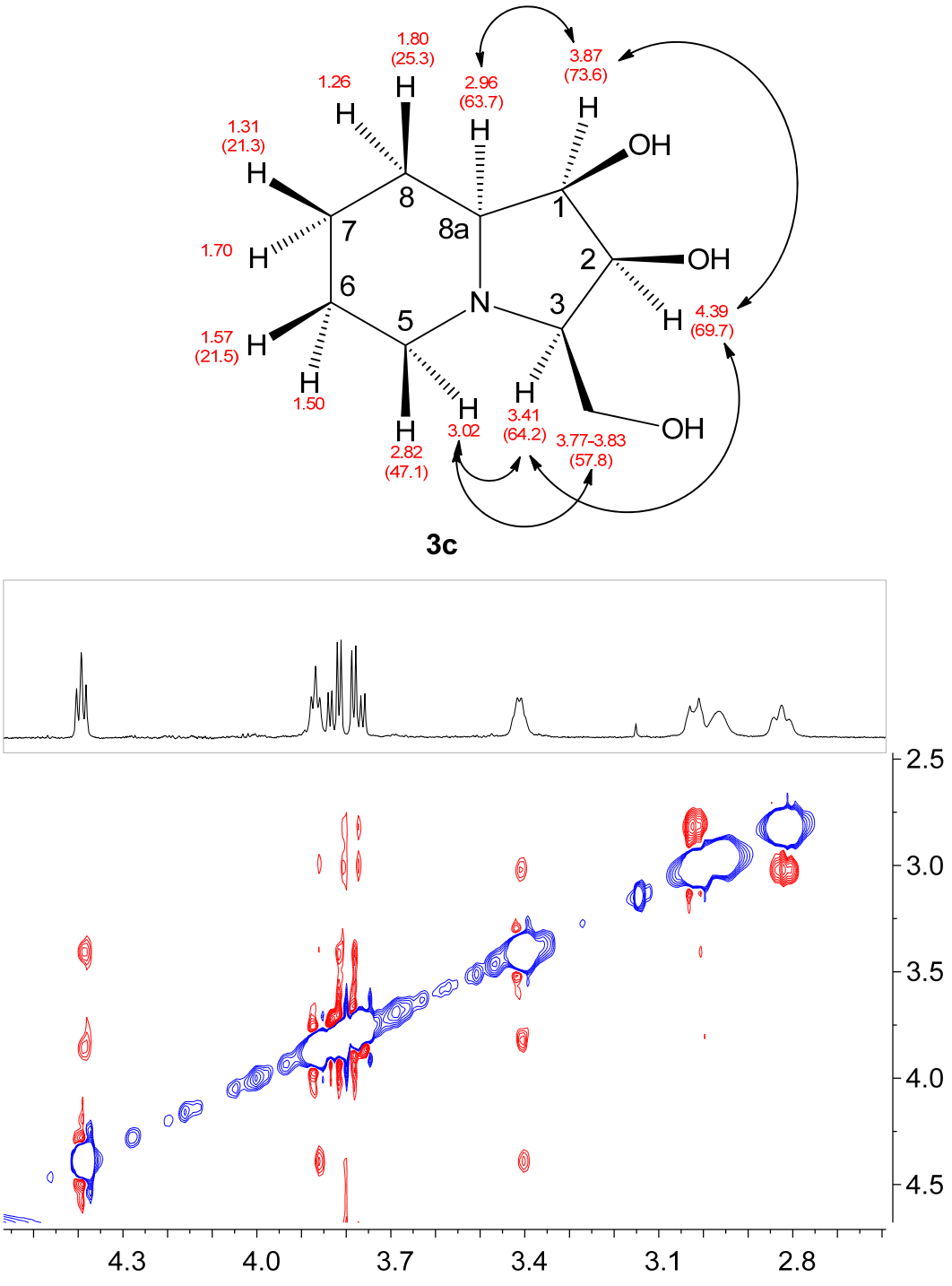

3c

Figure S4. Observed NMR spectra of **3d**: a) ^{1}H, b) 2D ^{1}H-^{1}H COSY and 2D multiplicity-edited HSQC, c) 2D NOESY and d) selective 1D NOESY spectra.

a)

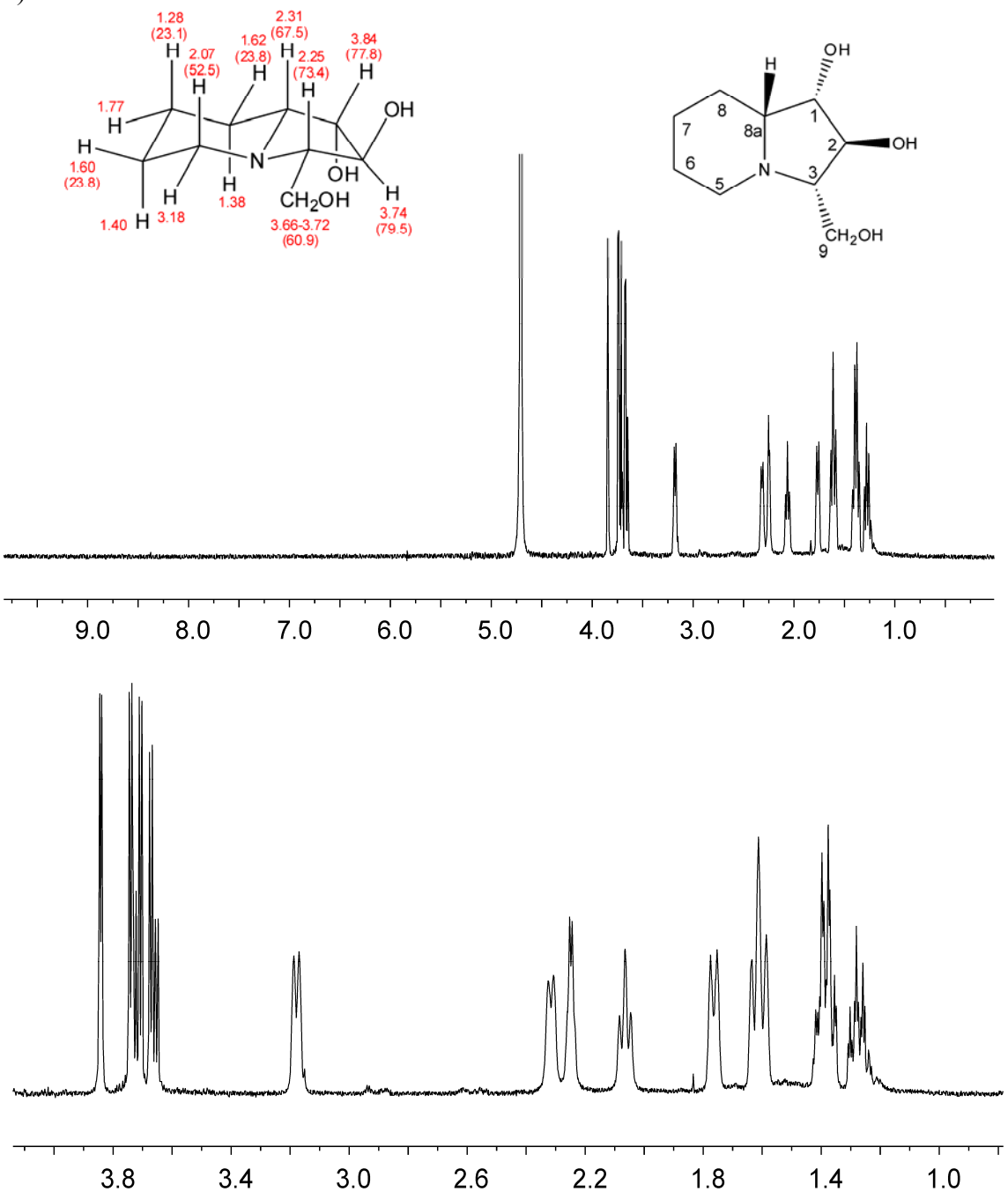

b)

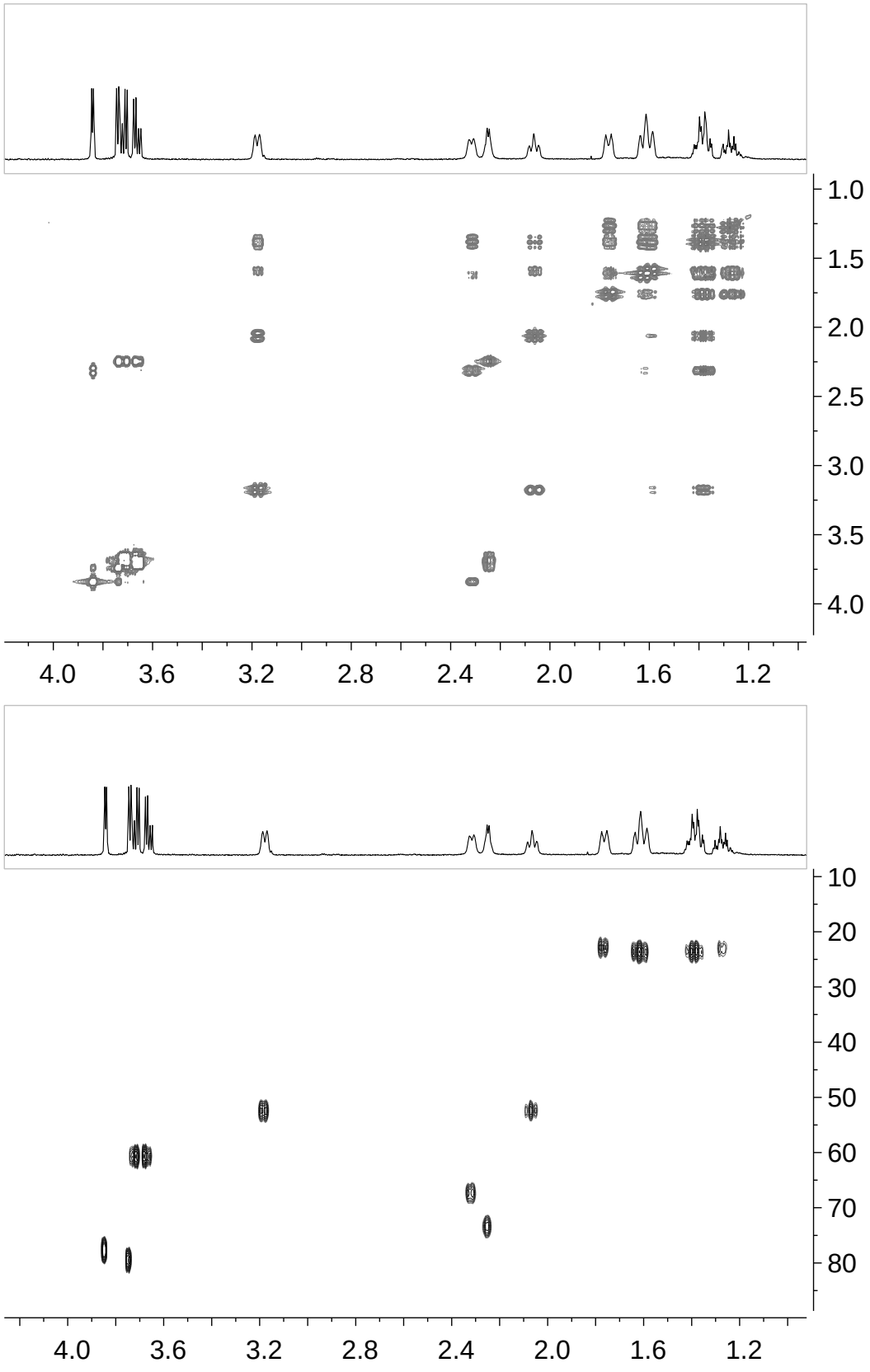

c)

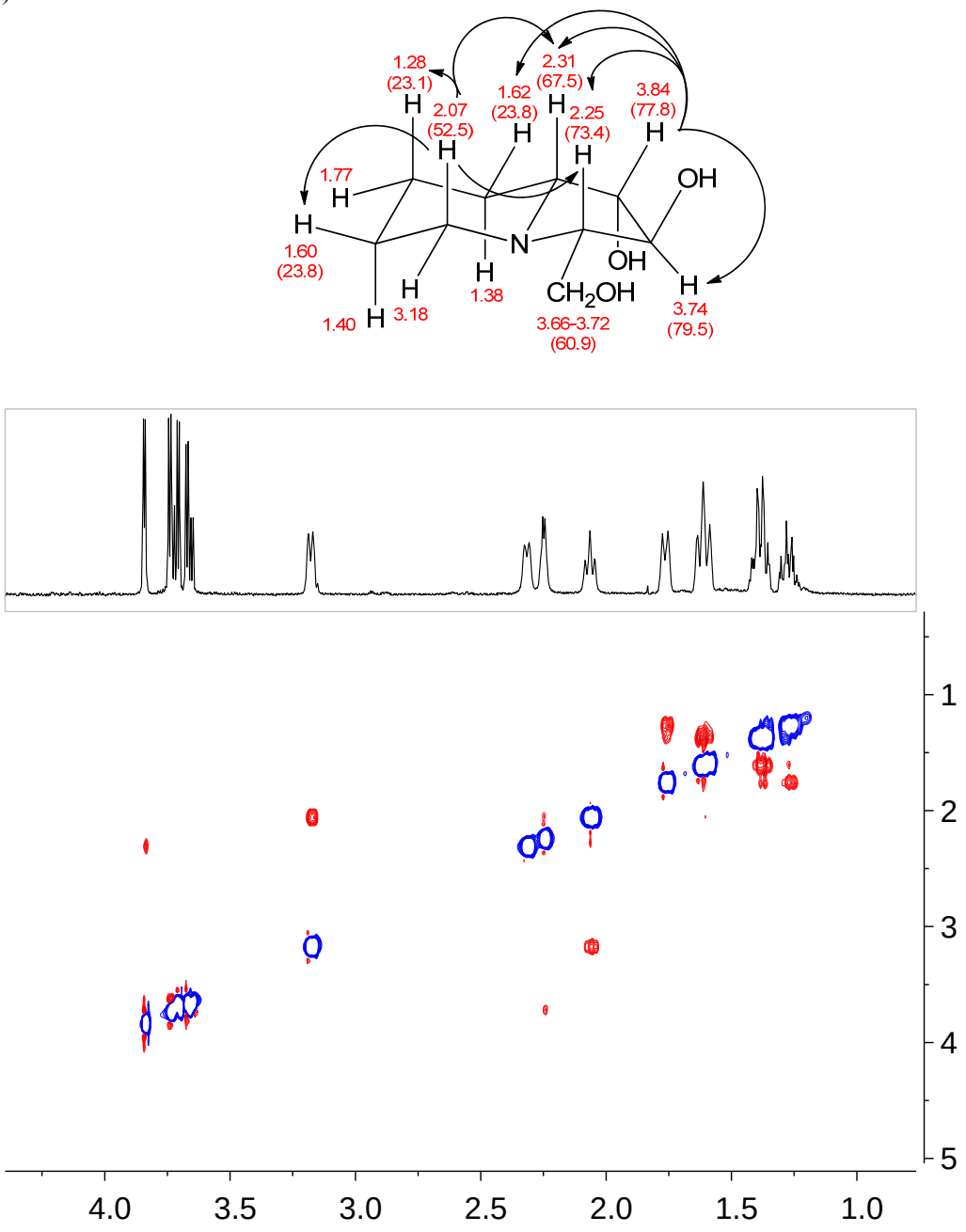
1.28
(23.1)
2.31
(67.5)
1.62
(23.8)
3.84
(77.8)
2.07
(52.5)
2.25
(73.4)
1.77
OH
1.60
(23.8)
N
OH
1.38
CH2OH
3.74
(79.5)
1.40
3.18
3.66-3.72
(60.9)
1
2
3
4
5
4.0
3.5
3.0
2.5
2.0
1.5
1.0

d)

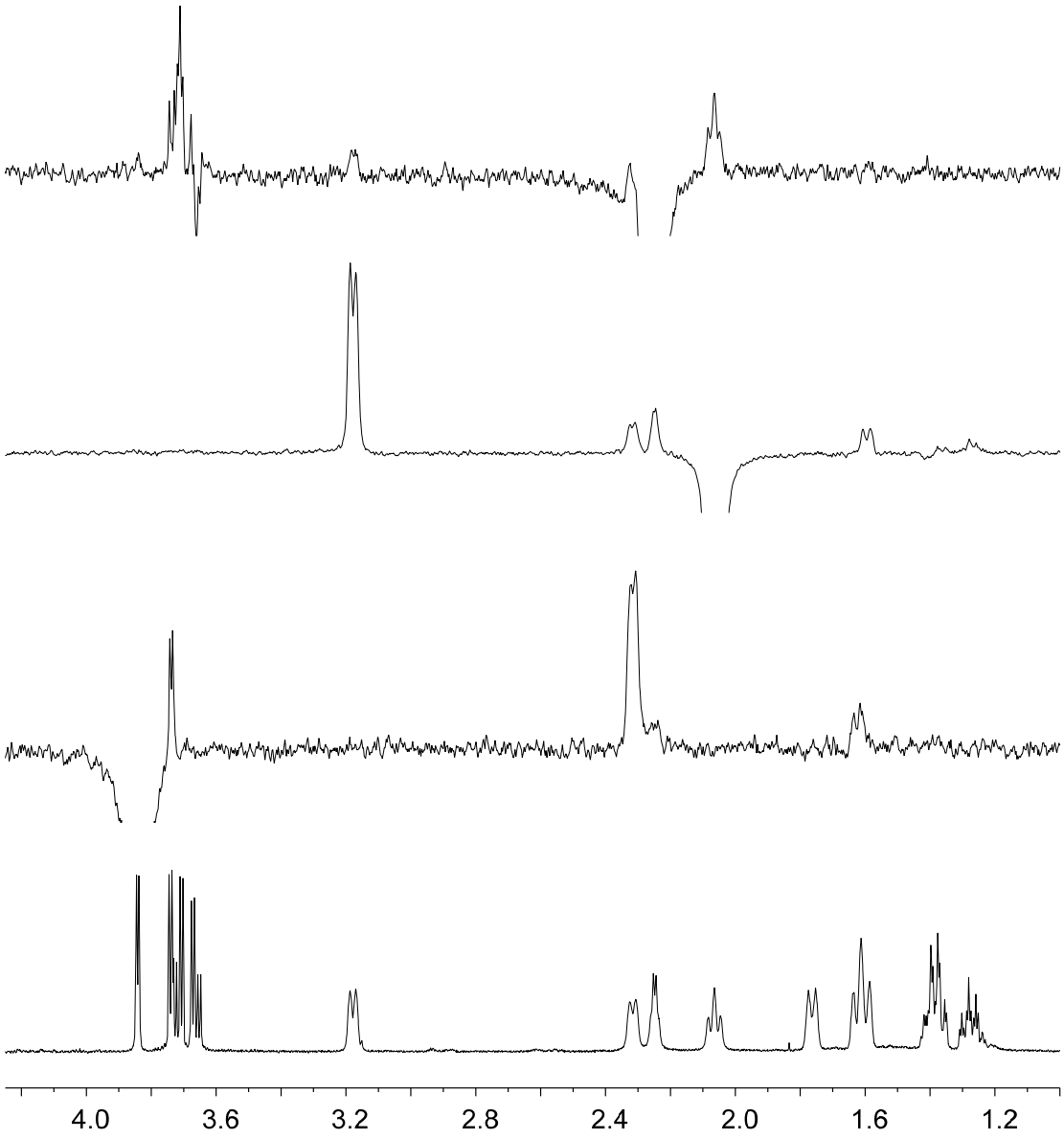

Figure S5. Observed NMR spectra of **3e**: a) ^{1}H, b) 2D ^{1}H-^{1}H COSY and 2D multiplicity-edited HSQC, c) 2D NOESY and d) selective 1D NOESY spectra.

a)

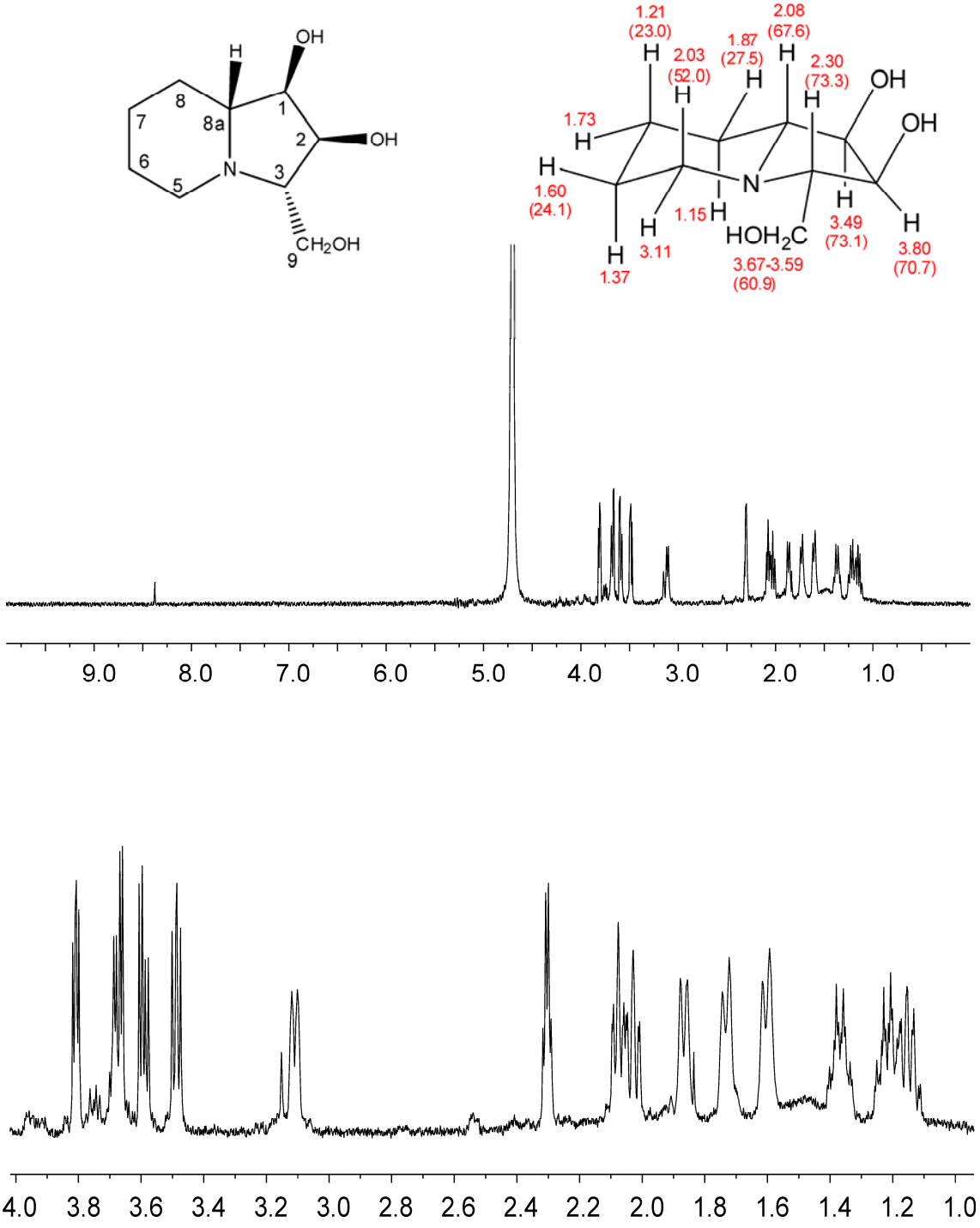

b)

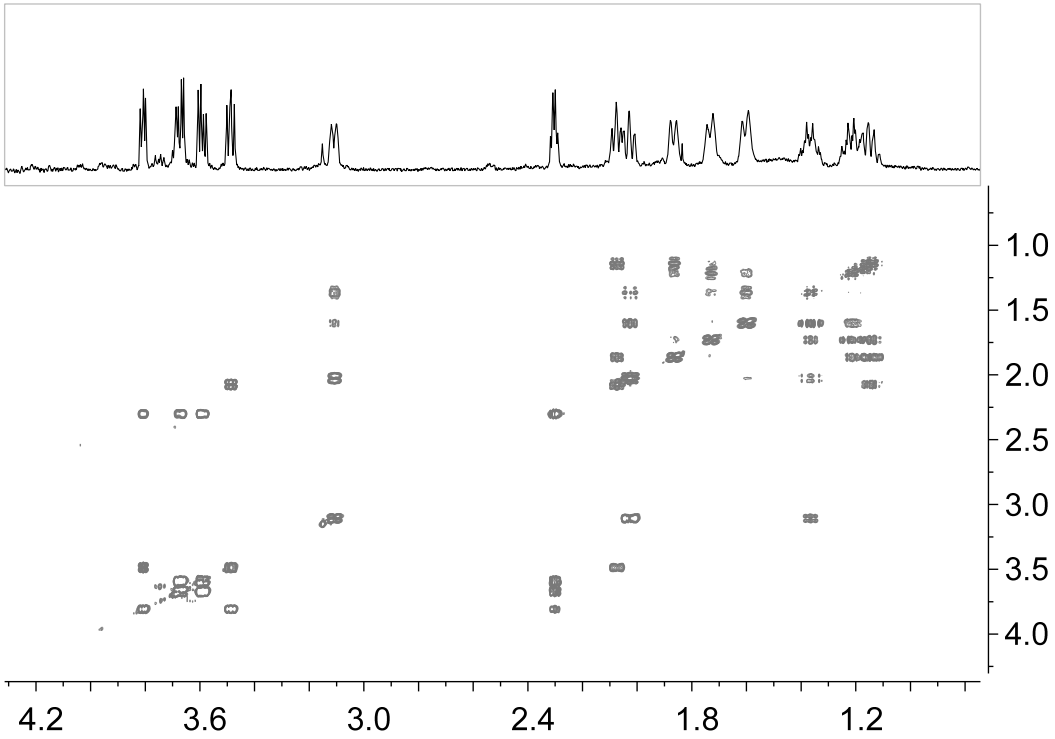

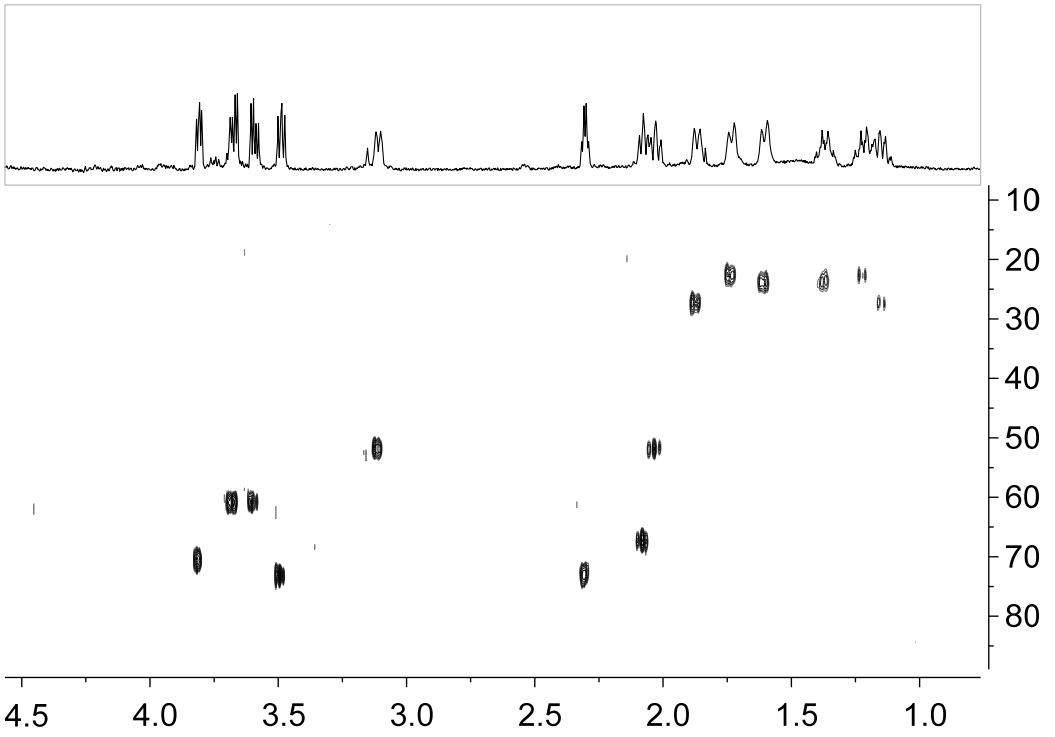

c)

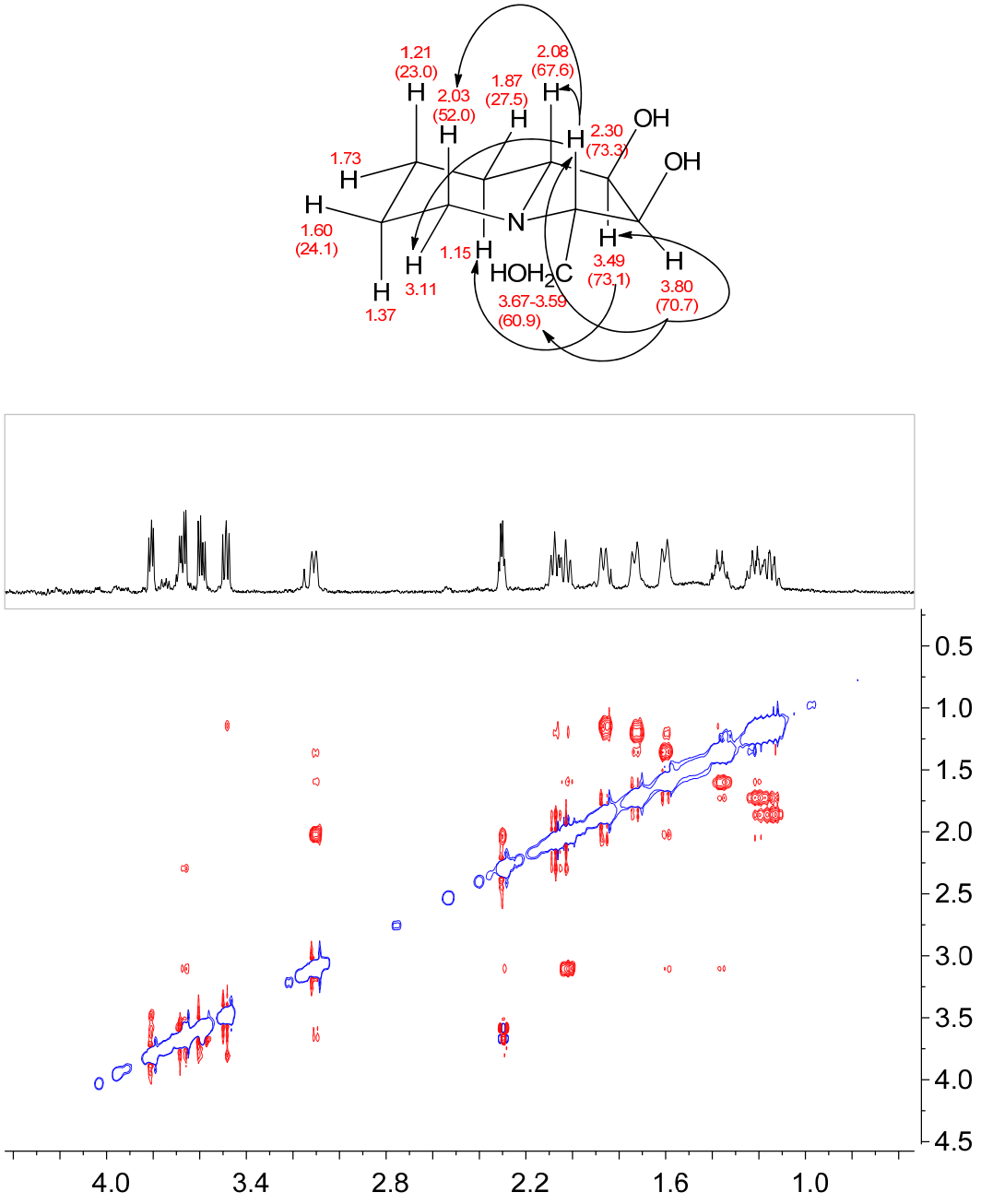
1.21
(23.0)
2.08
(67.6)
1.87
(27.5)
2.03
(52.0)
2.30
(73.3)
OH
OH
1.73
1.60
(24.1)
1.15
3.11
1.37
3.49
(73.1)
3.80
(70.7)
3.67-3.59
(60.9)
HOH2C
N
0.5
1.0
1.5
2.0
2.5
3.0
3.5
4.0
4.5
4.0
3.4
2.8
2.2
1.6
1.0

d)

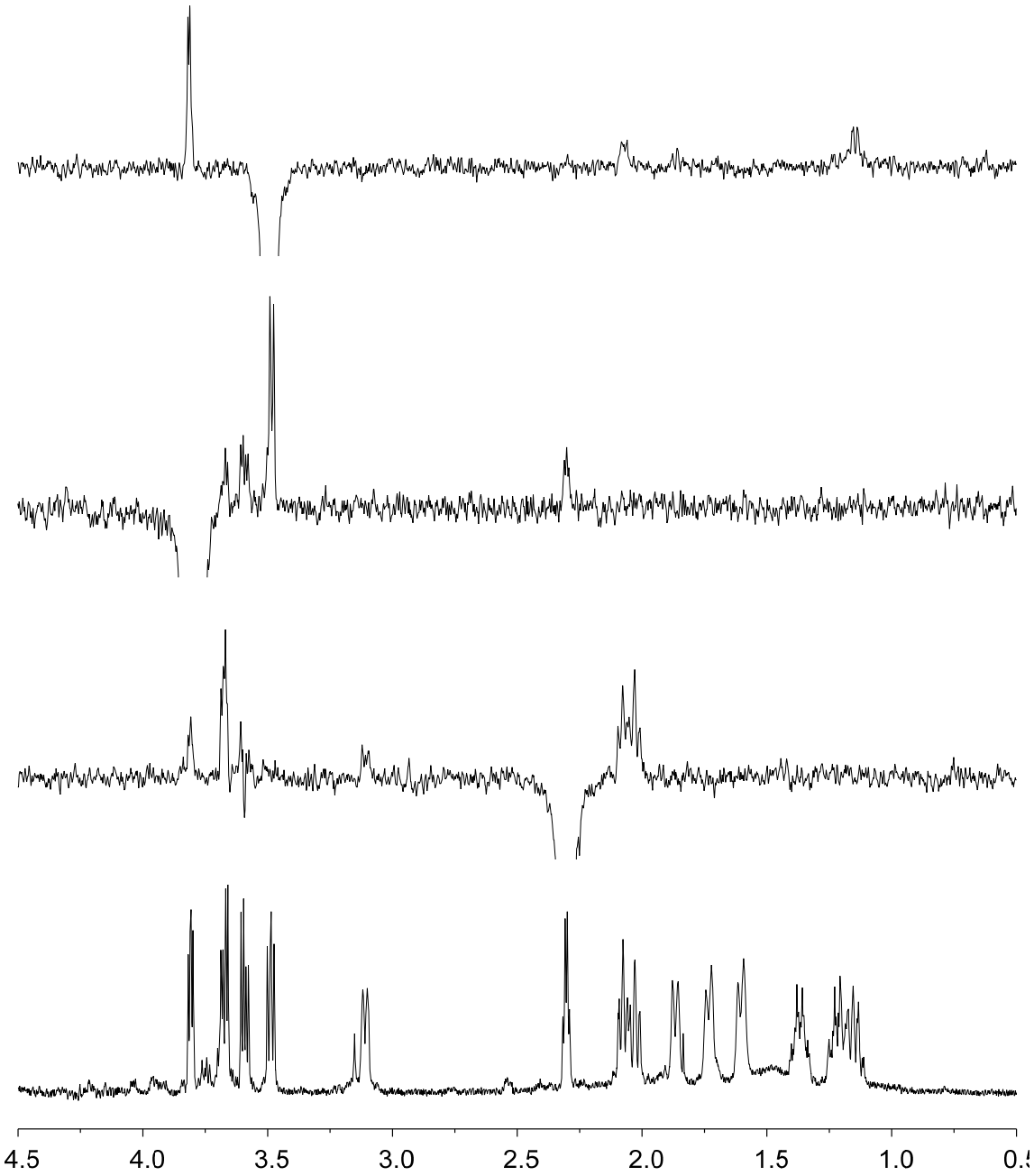

Figure S6. Observed NMR spectra of **4a**: a) ^{1}H, b) 2D ^{1}H-^{1}H COSY and 2D multiplicity-edited HSQC and c) 2D NOESY spectra.

a)

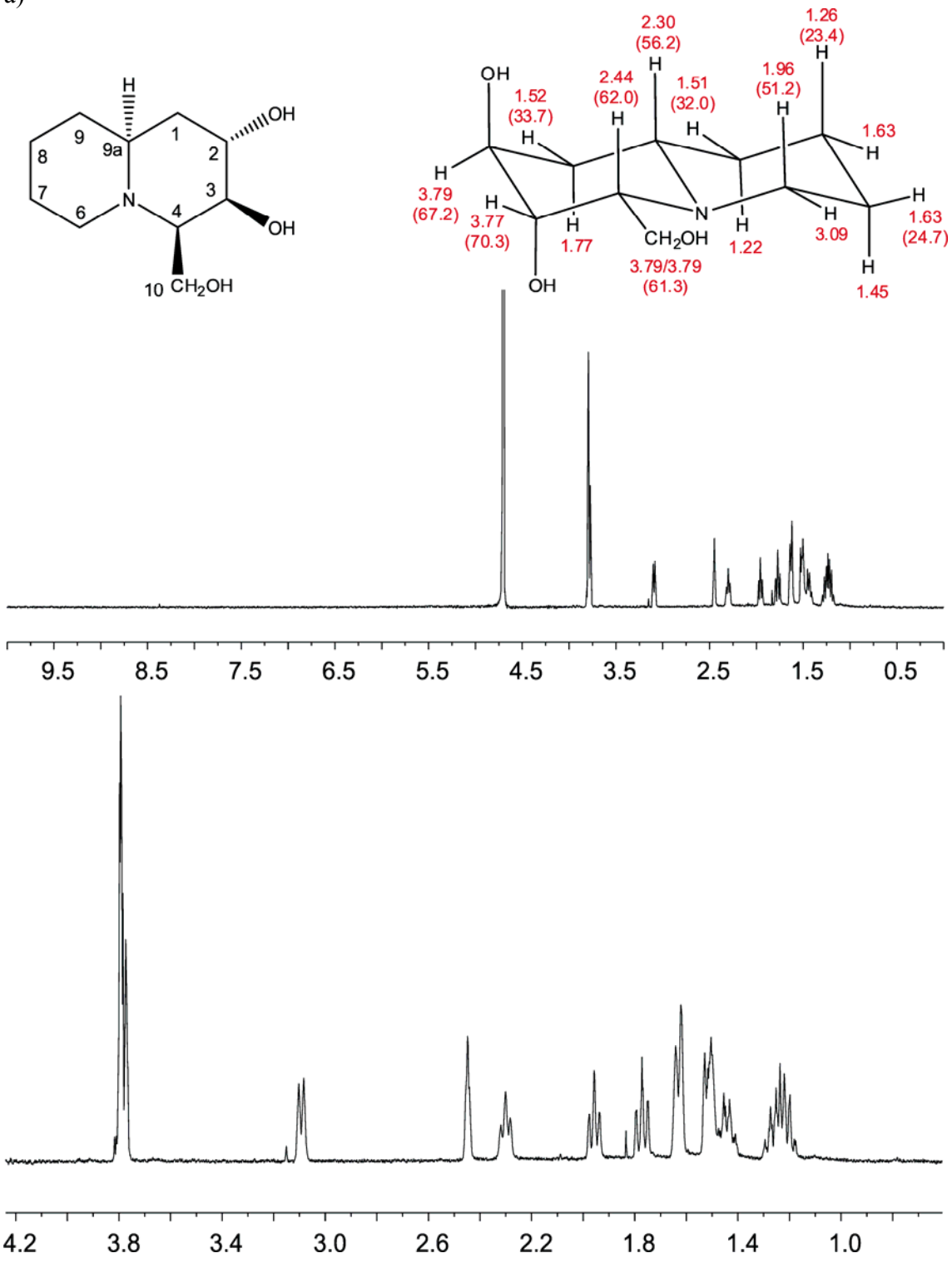

b)

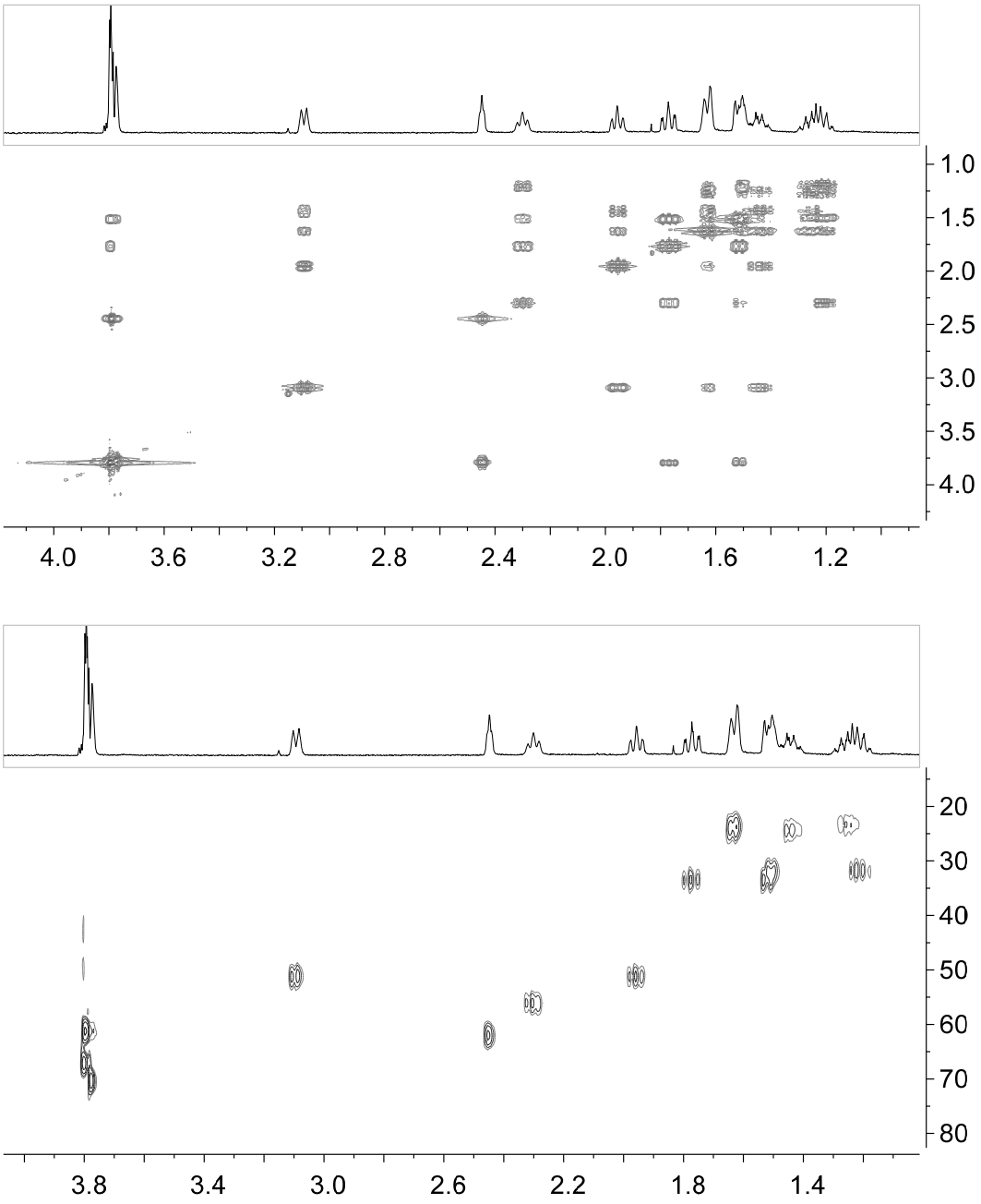

c)

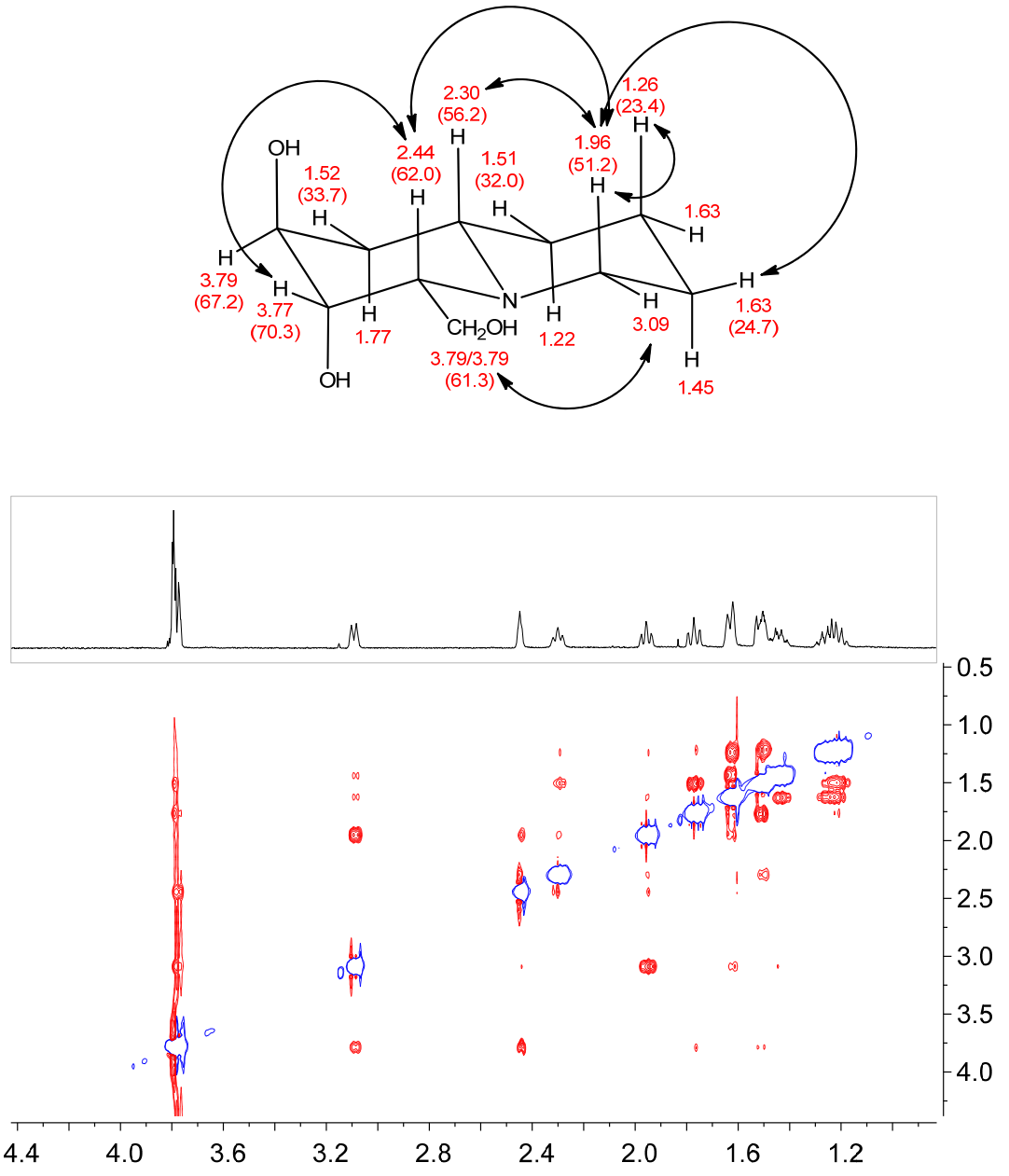
2.30
(56.2)
1.26
(23.4)
OH
2.44
(62.0)
1.96
(51.2)
1.52
(33.7)
1.51
(32.0)
1.63
3.79
(67.2)
3.77
(70.3)
1.77
CH2OH
1.22
3.09
1.63
(24.7)
3.79/3.79
(61.3)
1.45
OH
0.5
1.0
1.5
2.0
2.5
3.0
3.5
4.0
4.4
4.0
3.6
3.2
2.8
2.4
2.0
1.6
1.2

Figure S7. Observed NMR spectra of **4b** as mixture with compounds **4c** and **4f**: a) ^{1}H, b) 2D ^{1}H-^{1}H COSY and 2D multiplicity-edited HSQC and c) selective 1D NOESY spectra.

a)

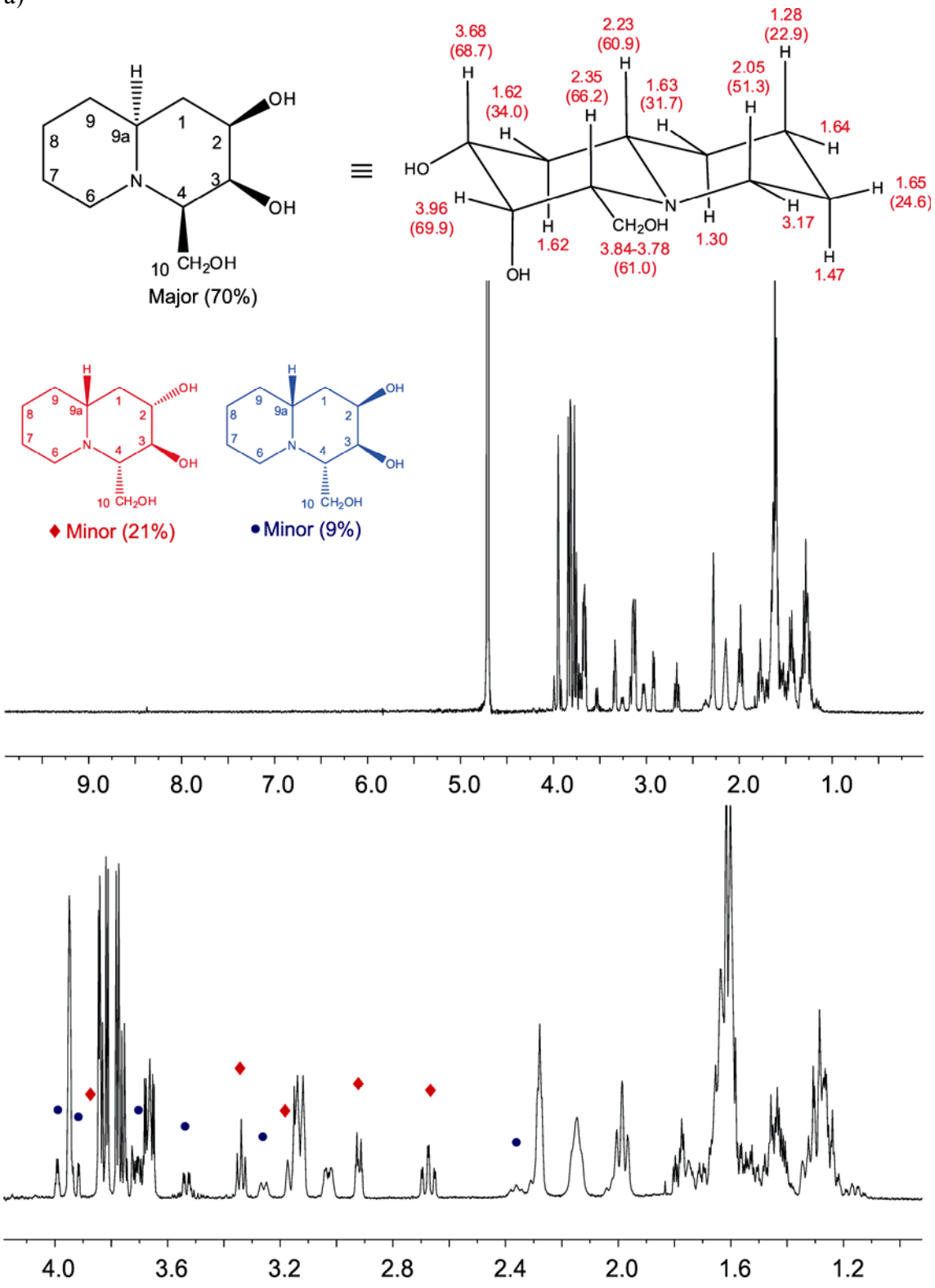

b)

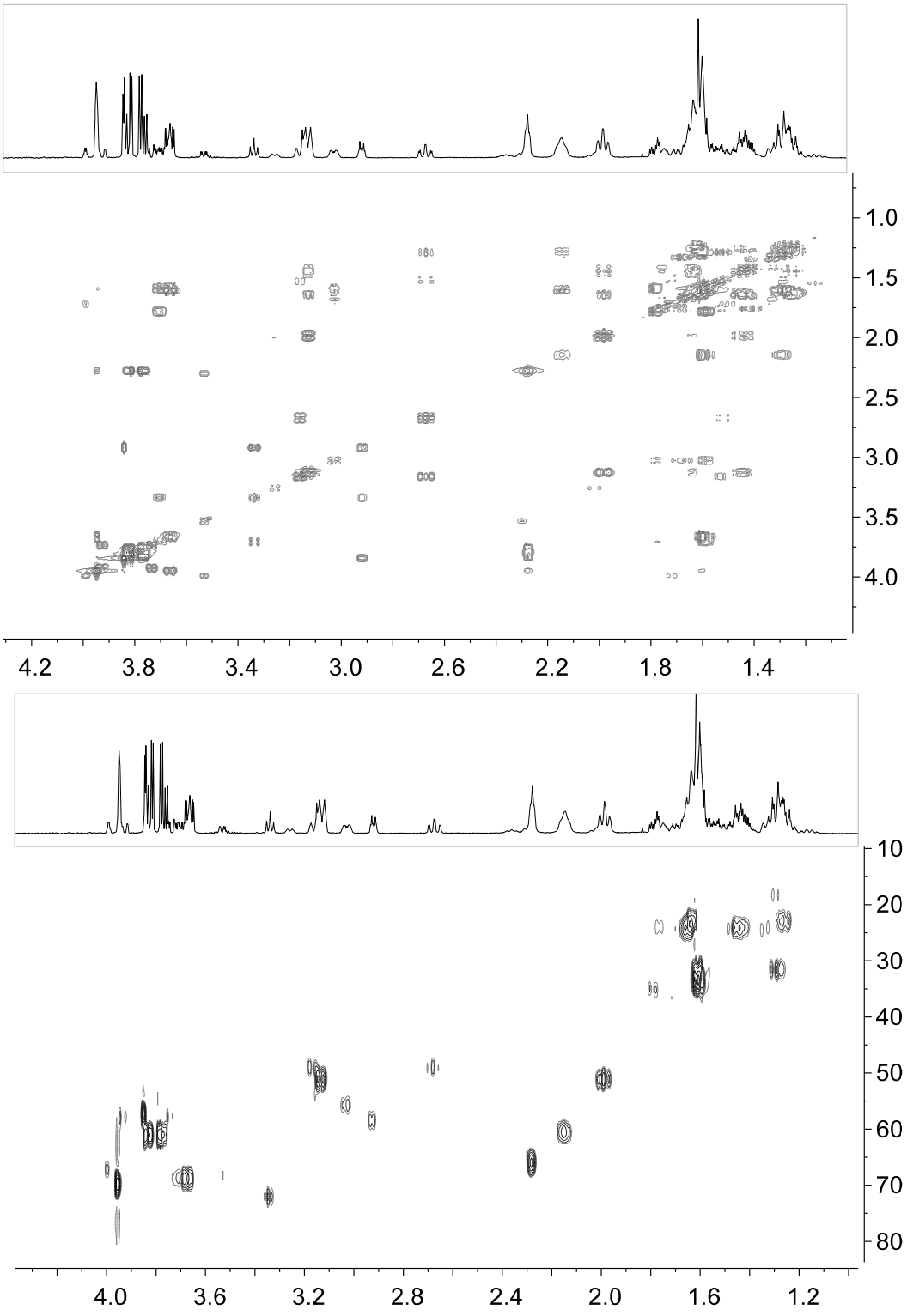
1.0
1.5
2.0
2.5
3.0
3.5
4.0
4.2
3.8
3.4
3.0
2.6
2.2
1.8
1.4
10
20
30
40
50
60
70
80
4.0
3.6
3.2
2.8
2.4
2.0
1.6
1.2

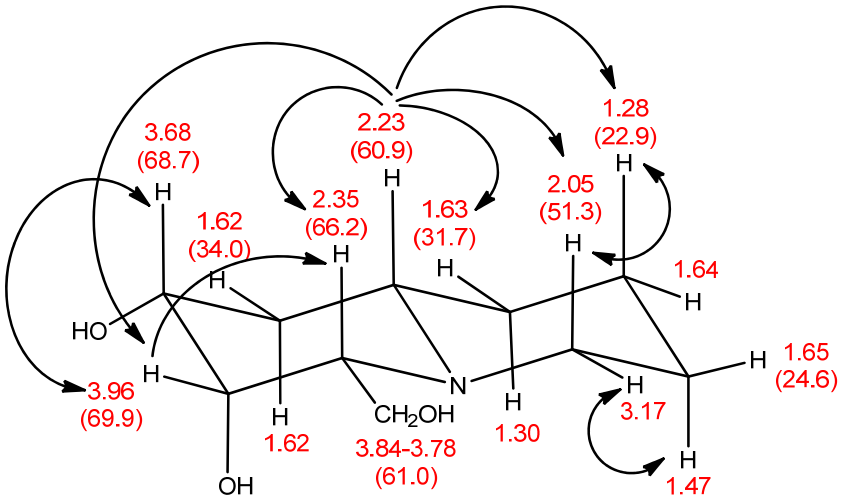

nOe's relations deduced from the NOESY spectra of Figure 8 (spectra mixture of compounds **4c** and **4b**.

Figure S8. Observed NMR spectra of **4c** as a mixture with compound **4b**: a) ^{1}H, b) 2D ^{1}H-^{1}H COSY and 2D multiplicity-edited HSQC, c) 2D NOESY and d) selective 1D NOESY spectra.

a)

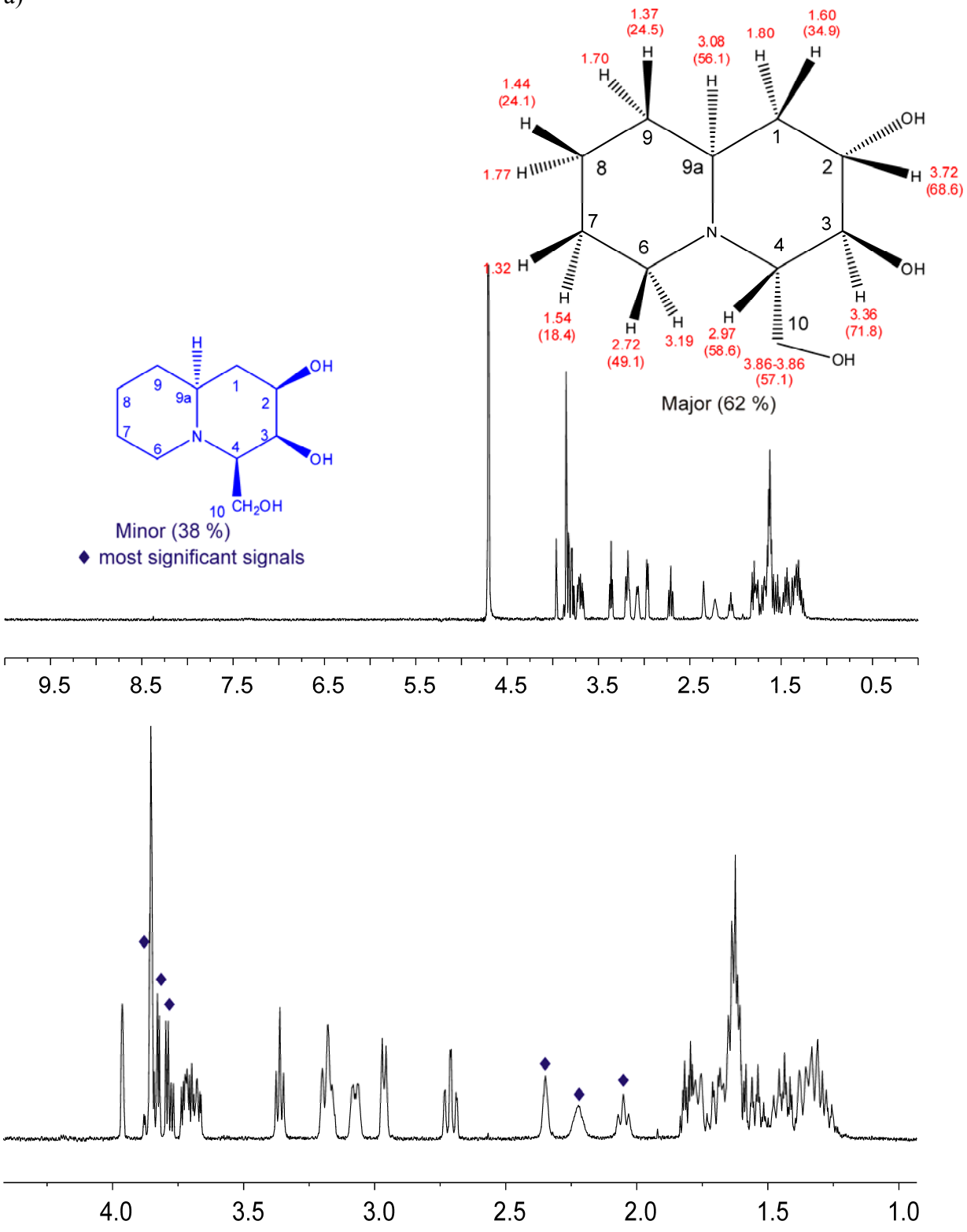

b)

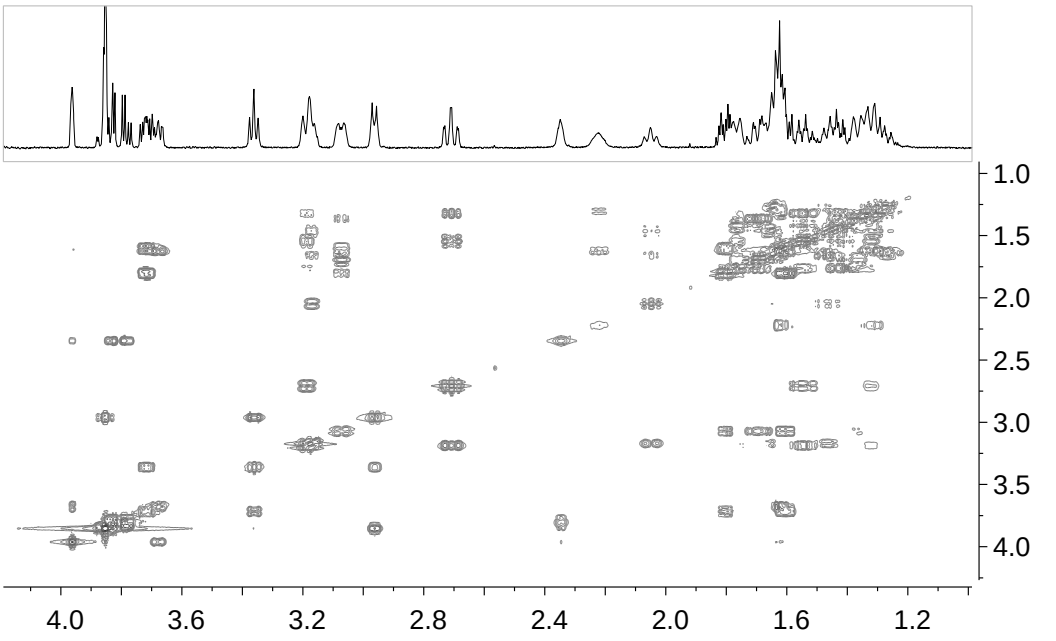

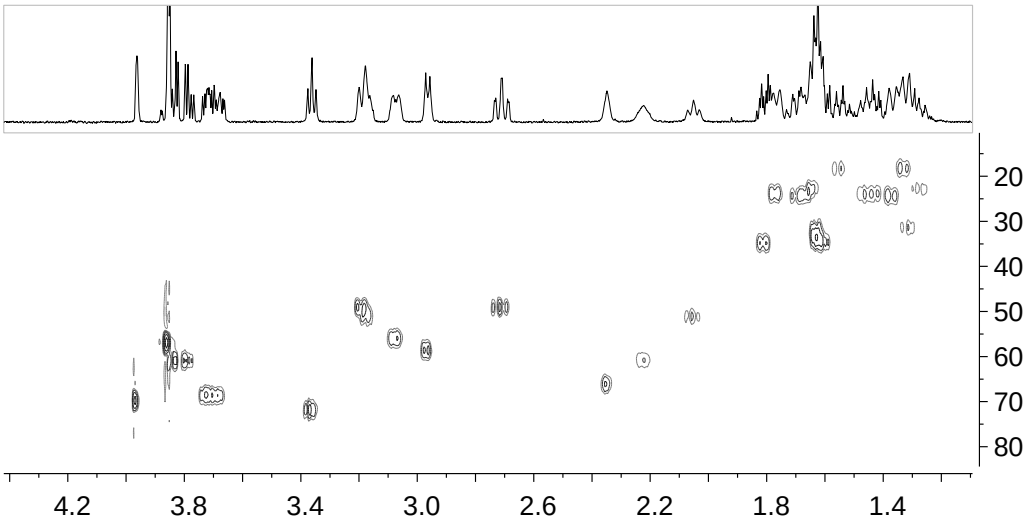

c)

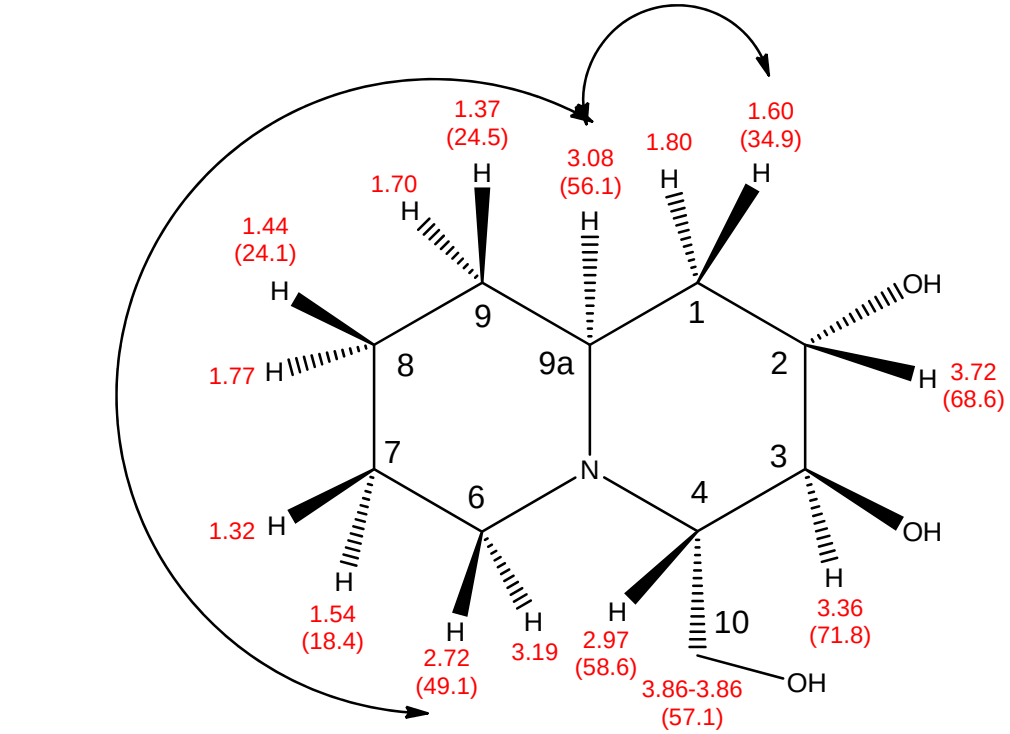

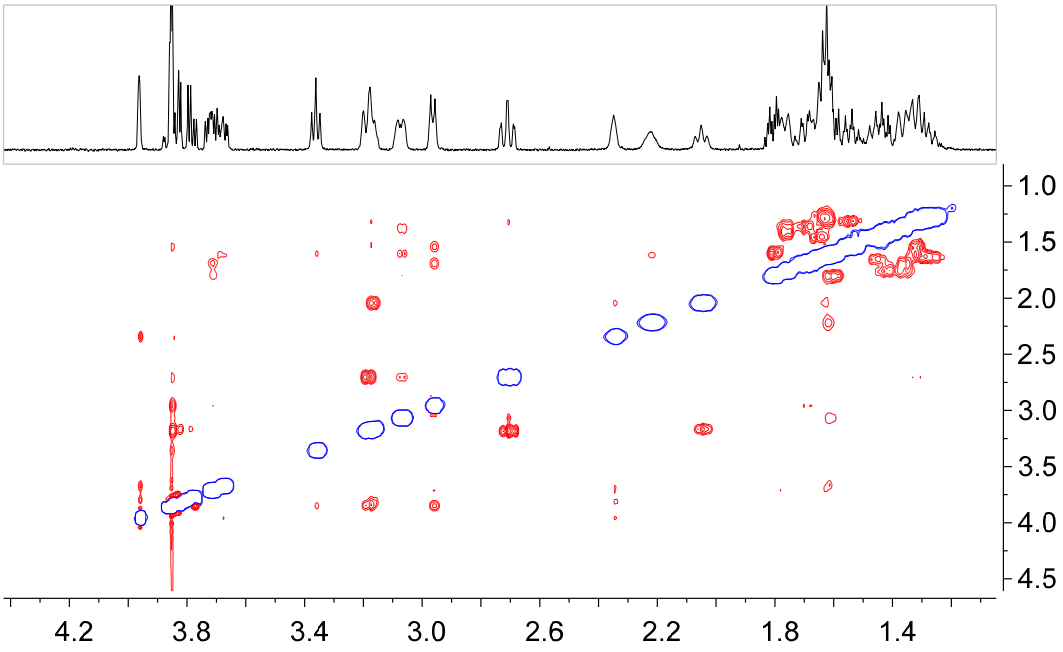

d)

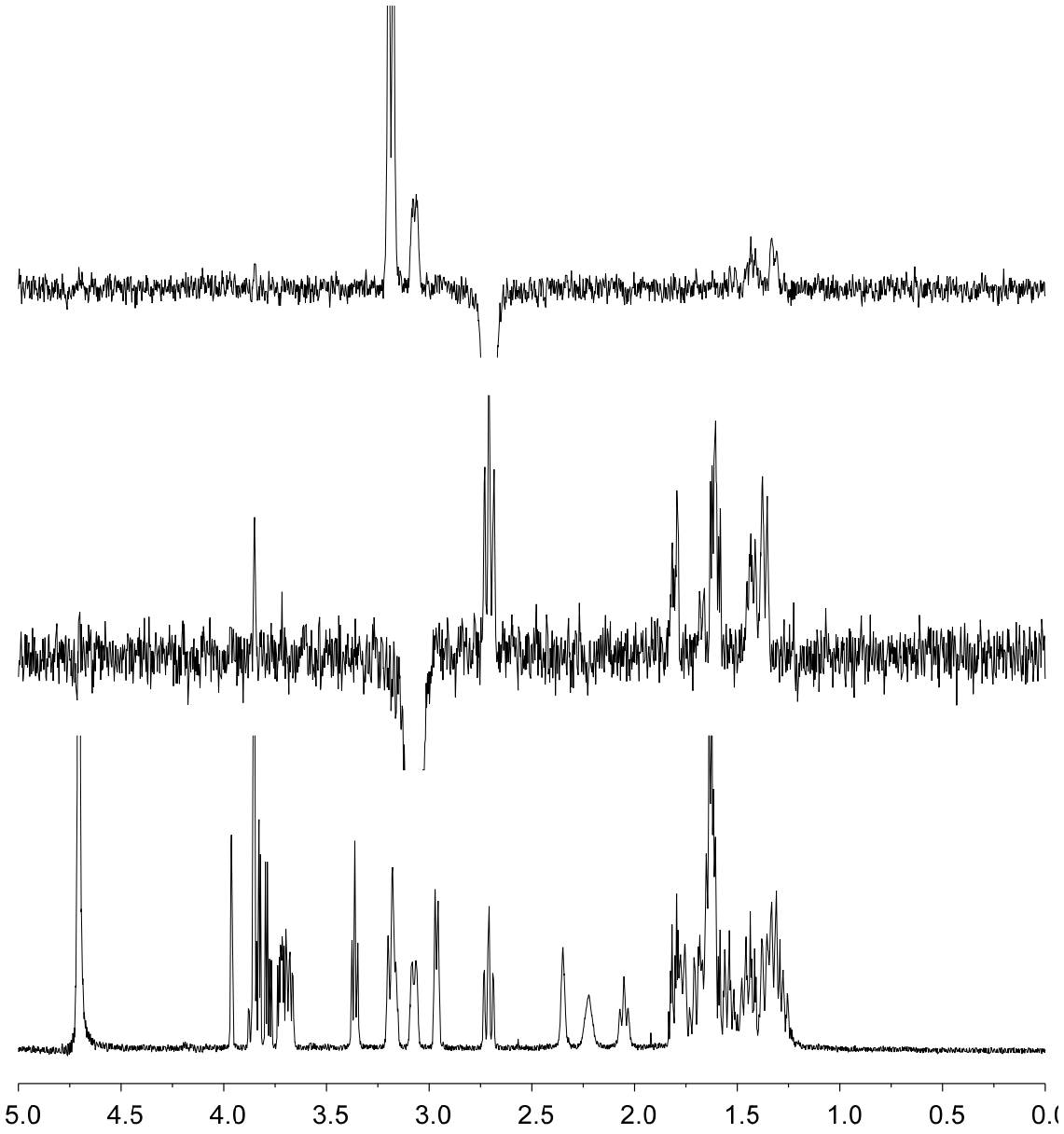

Figure S9. Observed NMR spectra of **4d**: a) ^{1}H, b) 2D ^{1}H-^{1}H COSY and 2D multiplicity-edited HSQC, c) selective 1D NOESY spectra.

a)

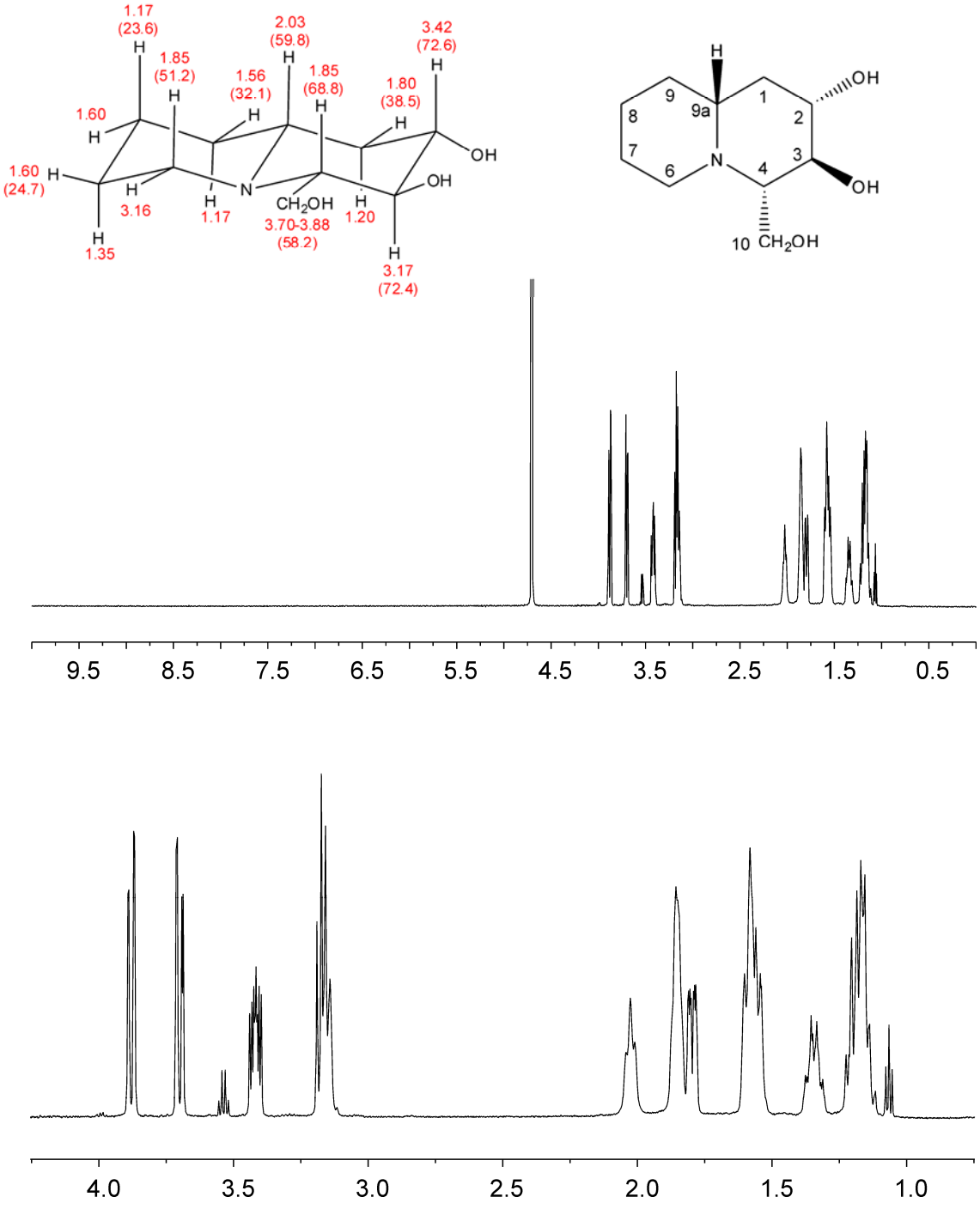

b)

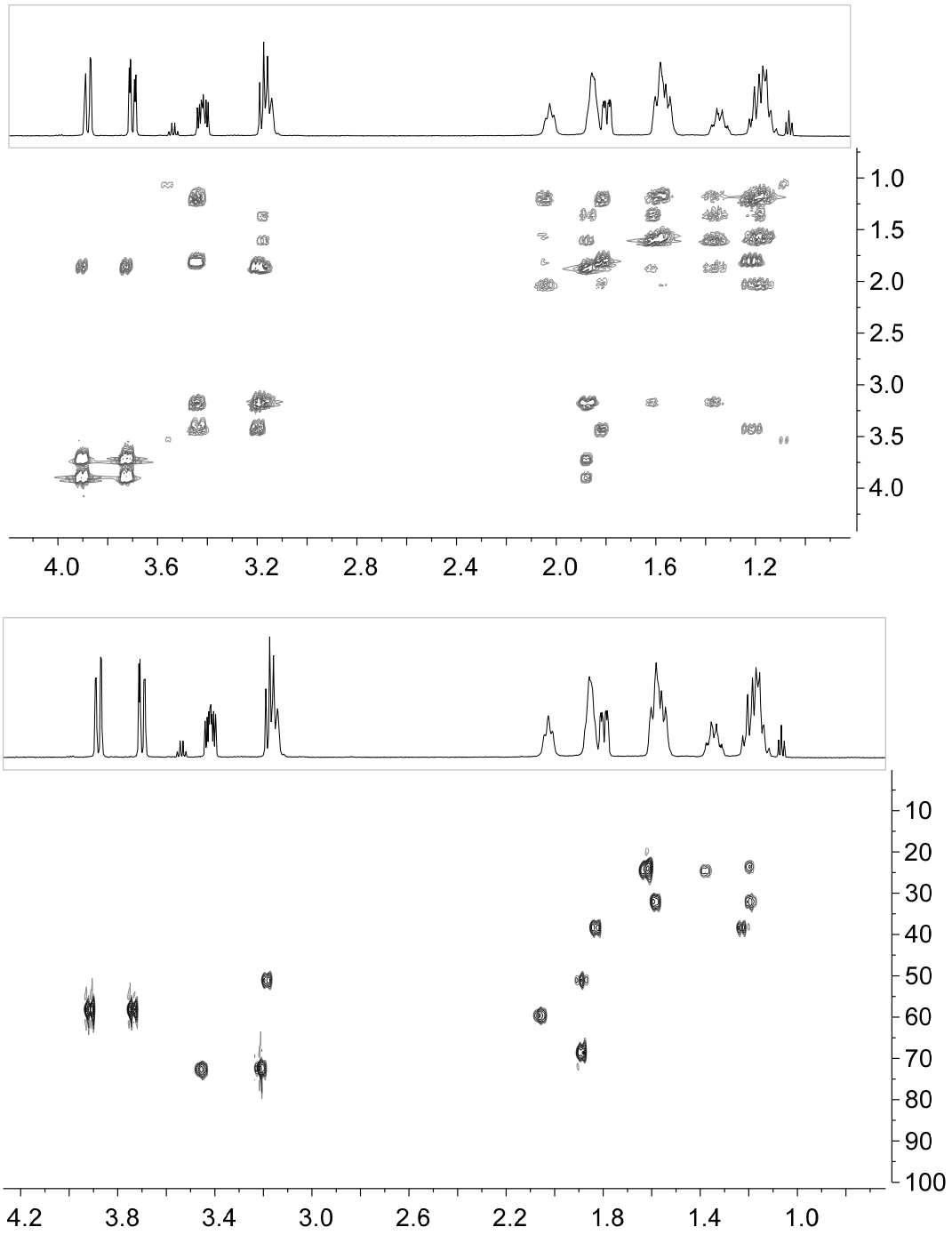
1.0
1.5
2.0
2.5
3.0
3.5
4.0
4.0
3.6
3.2
2.8
2.4
2.0
1.6
1.2
10
20
30
40
50
60
70
80
90
100
4.2
3.8
3.4
3.0
2.6
2.2
1.8
1.4
1.0

c)

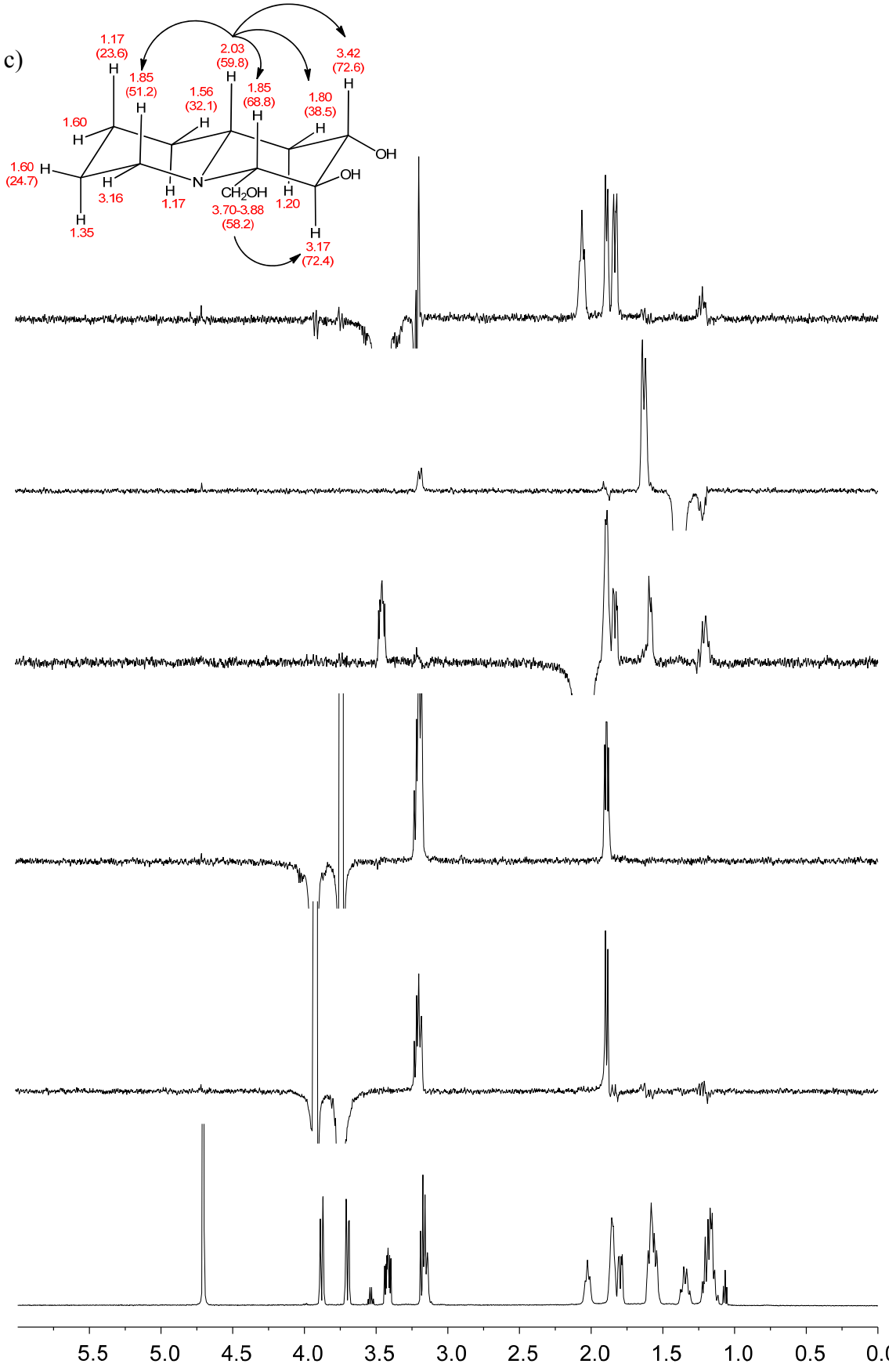

Figure S10. Observed NMR spectra of **4e**: a) ^{1}H, It was assigned using the NMR spectra of the mixture of **4e** and **4f** (see Figure 11).

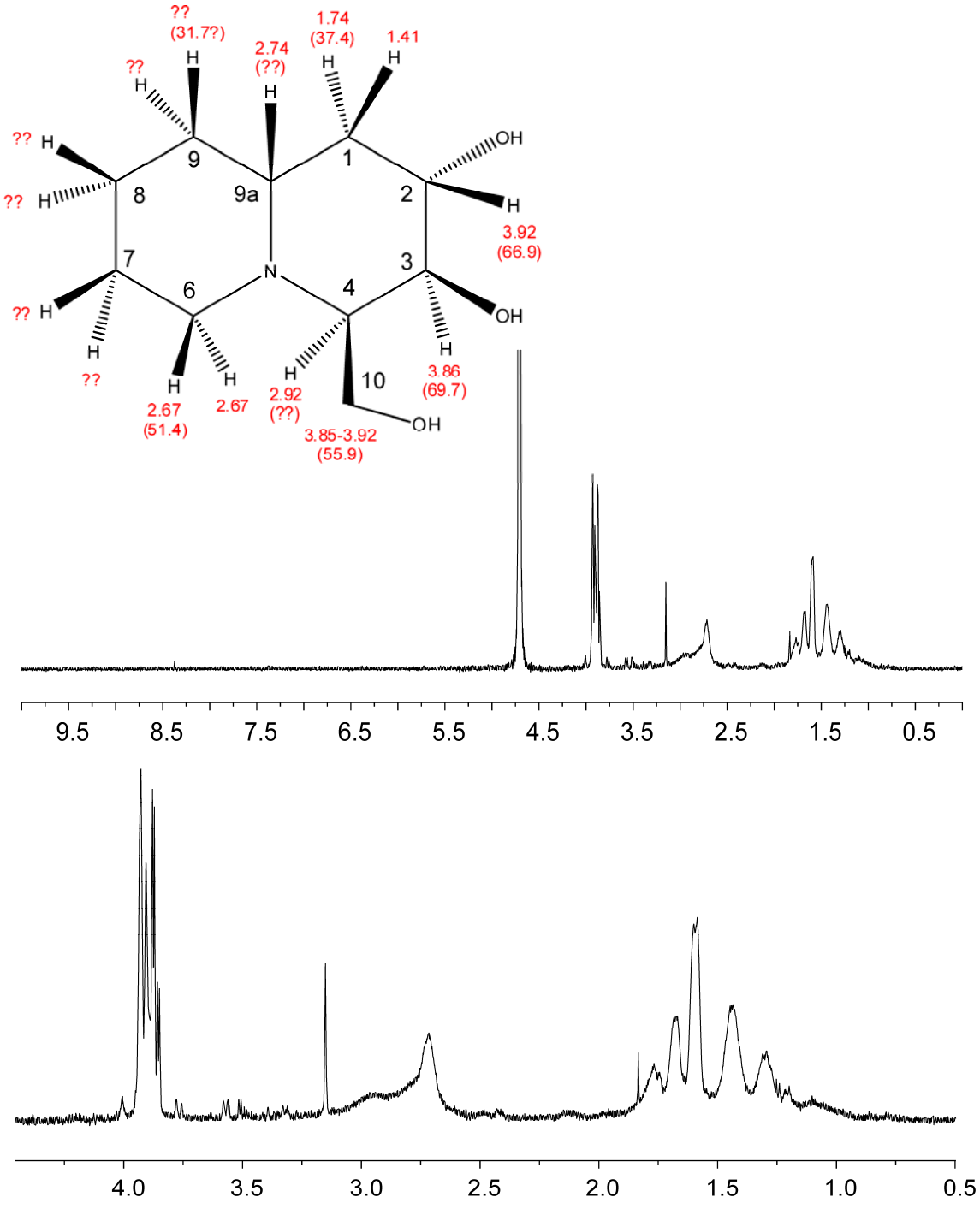

Figure S11. Observed NMR spectra of **4f** containing **4e** (1:1): a) ^{1}H, b) 2D ^{1}H-^{1}H COSY and 2D multiplicity-edited HSQC, c) selective 1D NOESY spectra.

a)

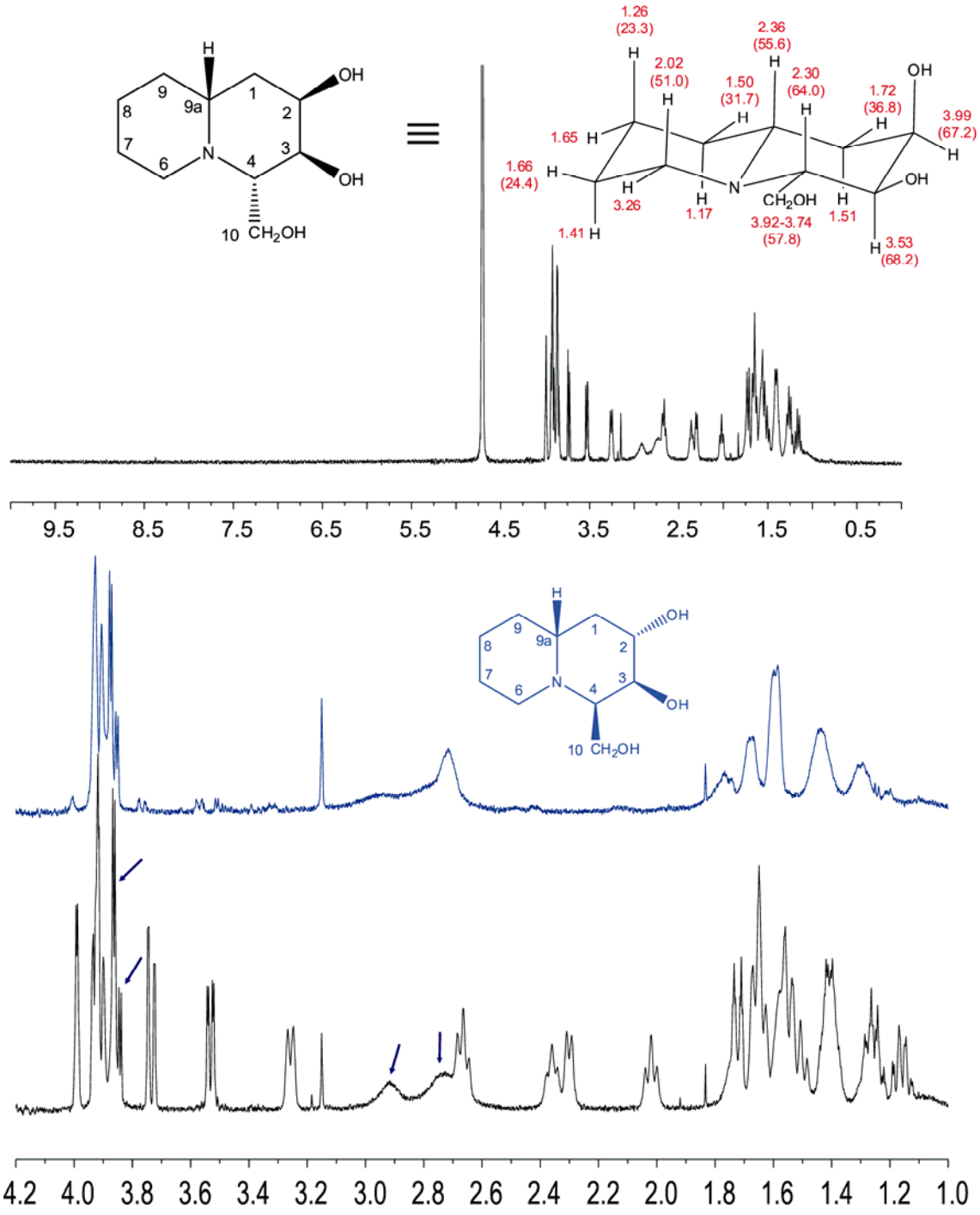

b)

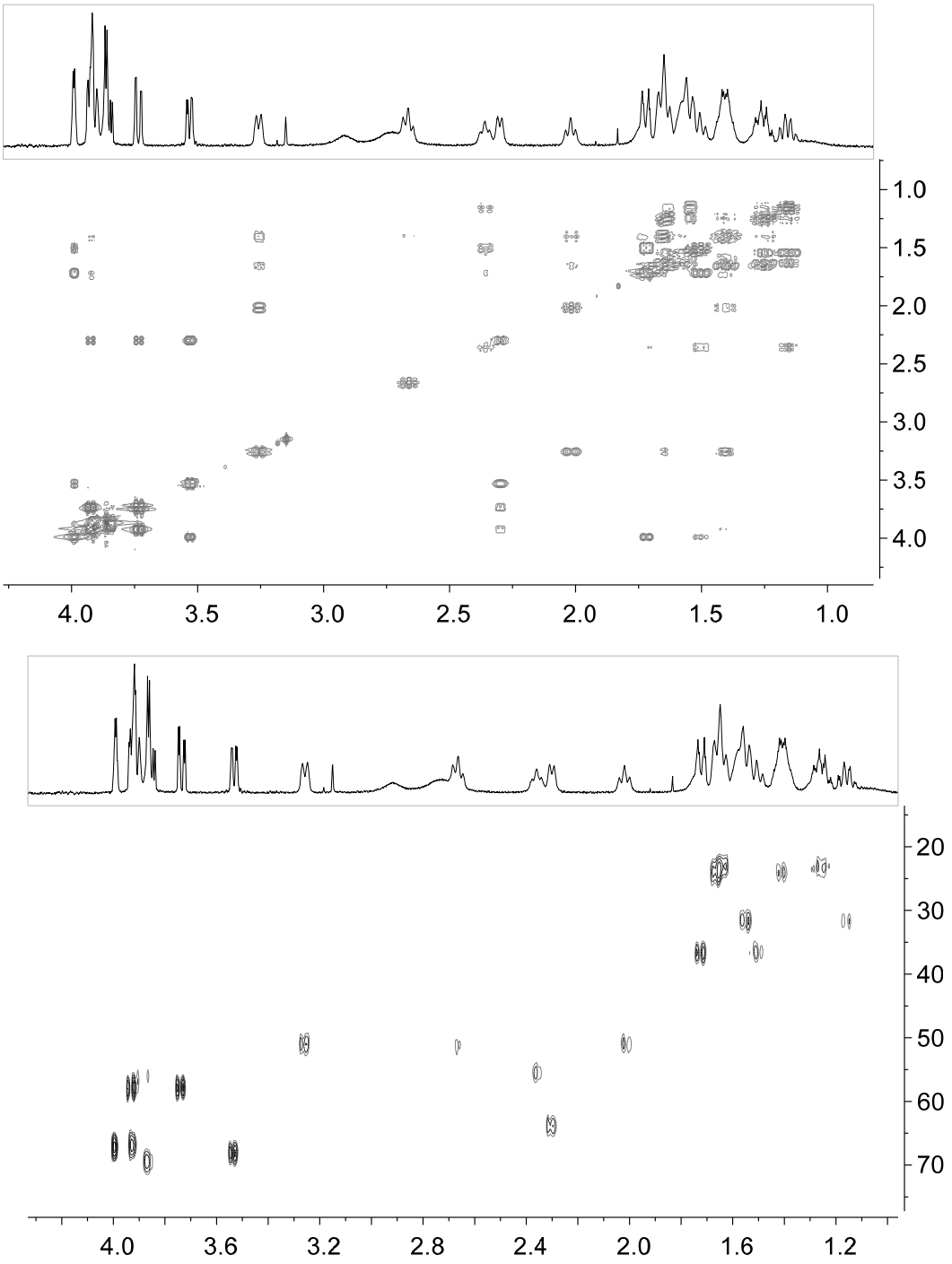

c)

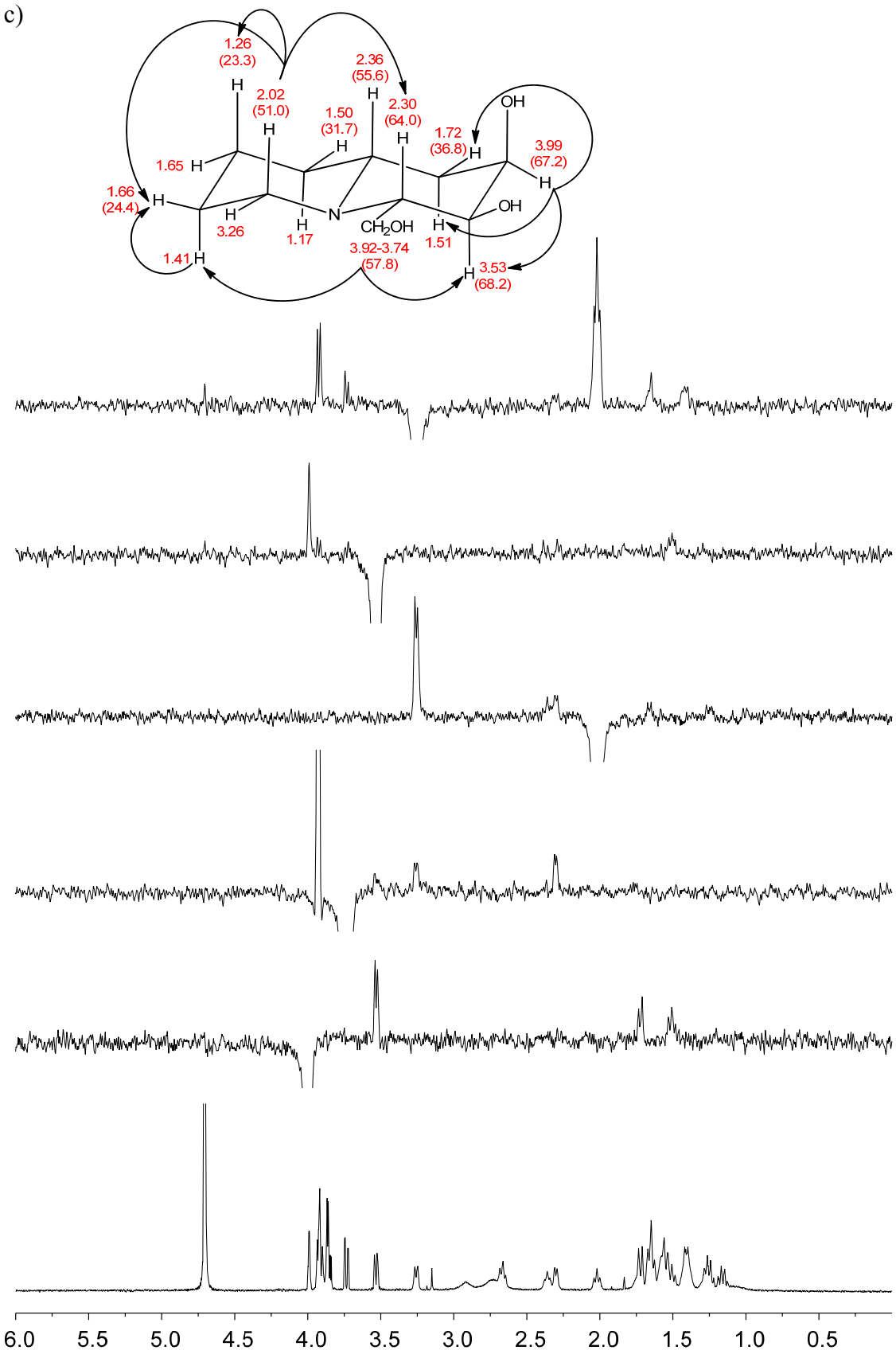

Figure S12. Observed ^{1}H NMR spectra of pure **4f**. The characterization was carried out on the spectra of Figure 11.

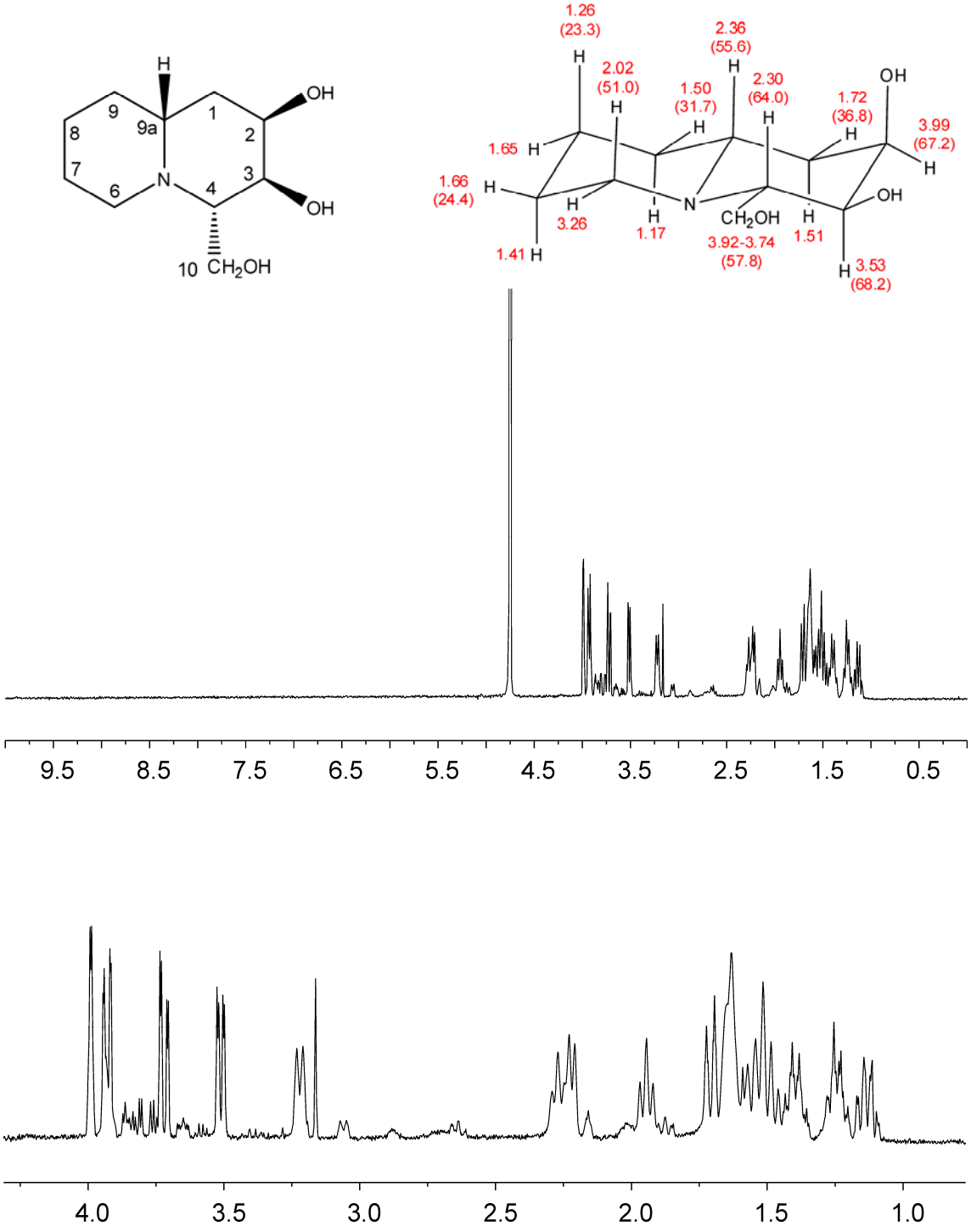

Table S1. Relevant NMR chemical shift values for indolizidine derivatives **3a-e** in D_2O.

Compound	δ(H8a)	δ(H3)	δ(H5/H5')	δ(C5)	δ(C1)	δ(C2)	δ(C9)
3a	1.89	2.54	3.07/1.97	52.1	81.7	75.3	58.3
3b	2.68	2.98	2.92/2.60	46.9	80.6	78.5	59.5
3c	2.96	3.41	3.02/2.82	47.1	73.6	69.7	57.8
3d	2.31	2.25	3.18/2.07	52.5	77.8	79.5	60.9
3e	2.08	2.30	3.11/2.03	52.0	73.1	70.7	60.9

Table S2. Relevant NMR parameters for quinolizidine derivatives **4a-f** in D_2O.

Compound	δ(H9a)	δ(H4)	δ(H6/H6')	δ(C6)	δ(C9)	δ(C10)
4a	2.30	2.44	3.09/1.96	51.2	32.0	61.3
4b	2.23	2.35	3.17/2.05	51.3	31.7	61.0
4c	3.08	2.97	3.19/2.72	49.1	24.5	57.1
4d	2.03	1.85	3.16/1.85	51.2	32.1	58.2
4e	2.74	2.92	2.67/2.67	~51.4	~31.7	55.9
4f	2.36	2.30	3.26/2.02	51.0	31.7	57.8

Figure S13. Lineweaver-Burk double reciprocal plots of **3a-e**, **4e** and **4f** inhibitions of α-L-rhamnosidase from *Penicillium decumbens*.

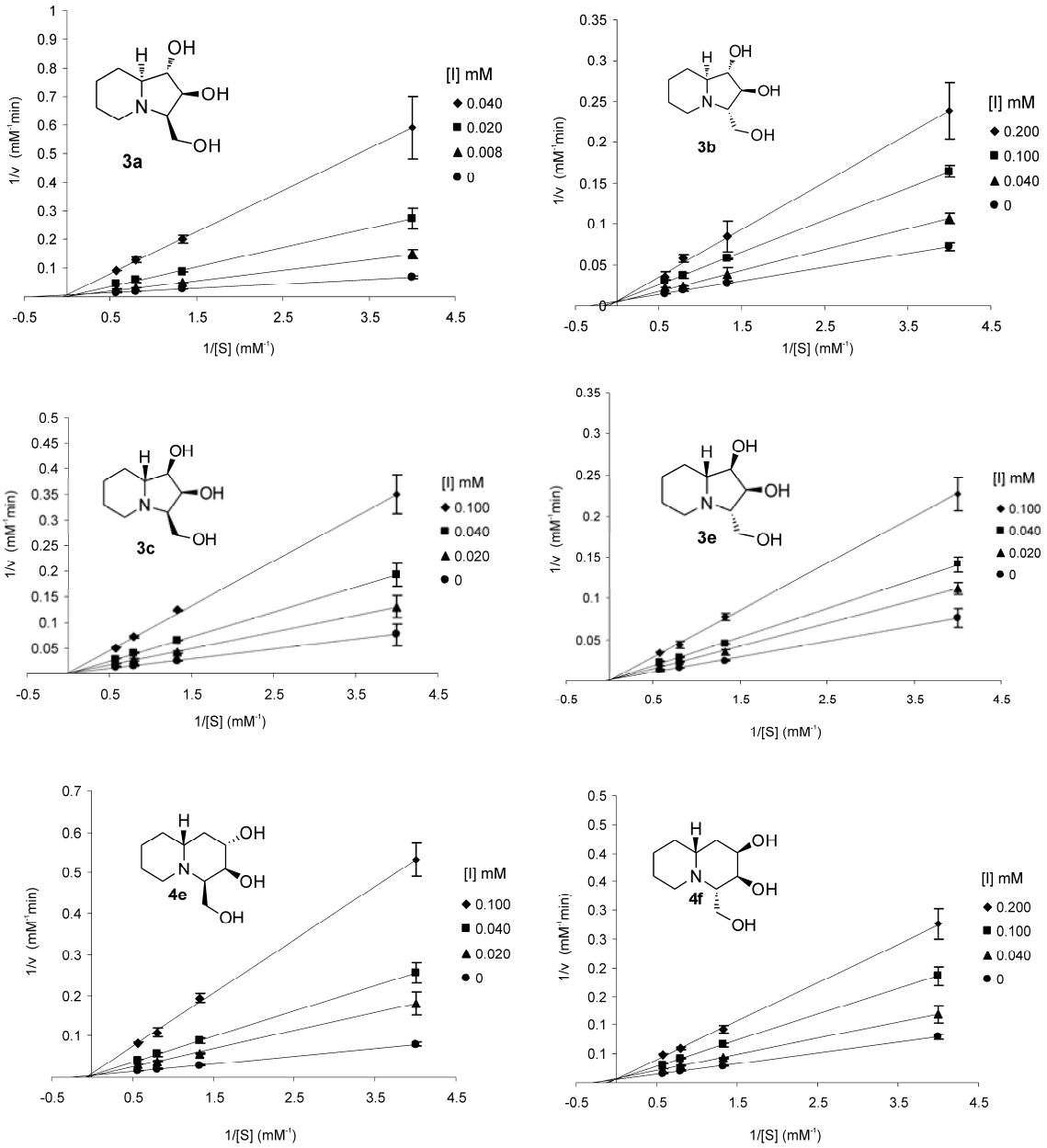

Figure S14. Lineweaver-Burk double reciprocal plots of **3c** inhibitions of α-L-fucosidase from bovine and α-L-mannosidase from jack beans**,** and **3b** inhibition of α-D-glucosidase from rice.

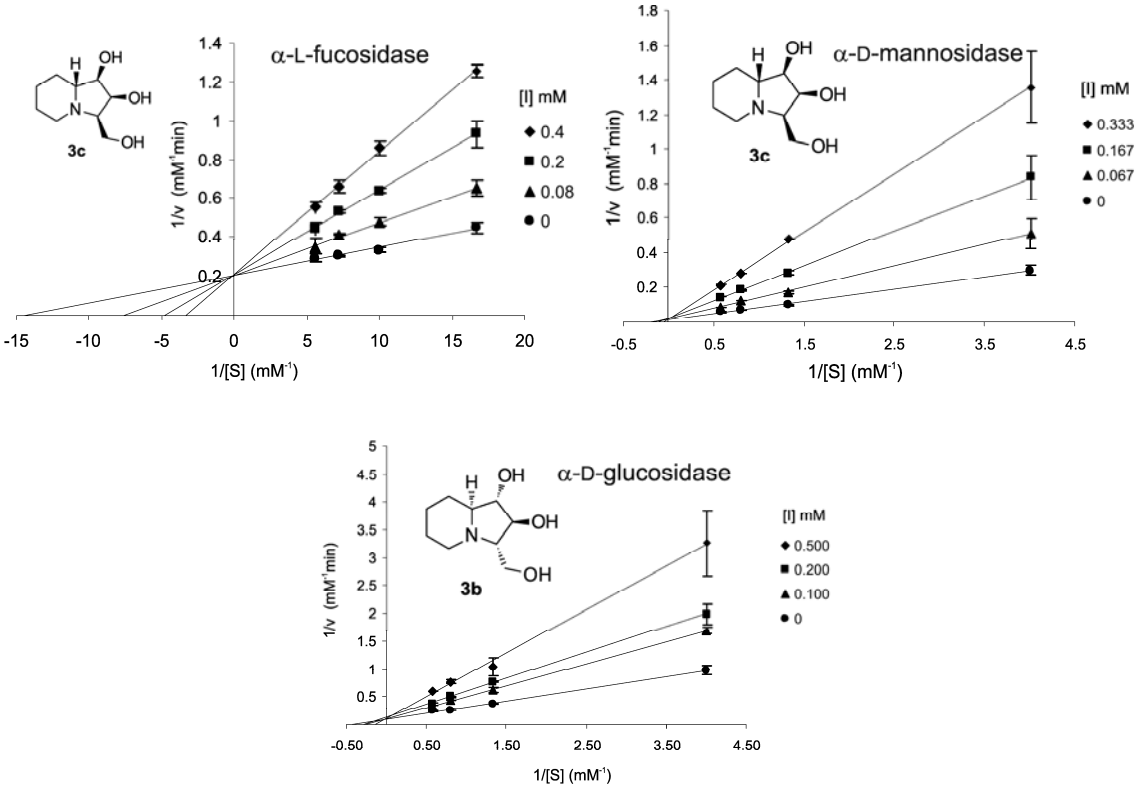

In silico conformational analysis

An *in silico* conformational analysis of compounds **3a-e** and **4a-f** was carried out by using density functional theory (DFT) calculations. For this purpose, an initial molecular mechanics conformational search was performed. Then, all the minima located for each compound were reminimized at the B3LYP/6-31G** level with implicit water solvation conditions and, finally, the energies in solution of all the new minima were recalculated using the larger basis set cc-pVTZ(-f). The same protocol was applied to two additional model compounds, 1-deoxycastanospermine (**DOC**) and 1-deoxy-8a-*epi*-castanospermine (**DOEC**), which have been reported to adopt $^{8}C_{5}$ and $^{5}C_{8}$ structures, respectively, in solution.[3]

Thus, the conformational analysis of **DOC** yielded 25 stereoisomers within 2.0 kcal mol^{-1} from the lowest energy minimum (Figure 15), which differed mainly in the orientation of the three equatorial hydroxyl groups, showing in all cases a *trans* ring fusion [4] and a $^{8}C_{5}$ chair conformation for the polyhydroxylated ring (Chart 1), in good agreement with the experimental observations.[3] On the other hand, **DOEC** yielded 33 structures within 5.0 kcal mol^{-1} from the lowest energy minimum (Figure 13). Among these, the most stable stereoisomer adopted a *trans*-$^{5}C_{8}$ disposition with three axial hydroxyl groups, while *cis*-$^{8}C_{5}$ conformations, appearing by inversion of the chair and the nitrogen atom and with the three hydroxyl groups in equatorial, were also detected at >1.0 kcal mol^{-1} above the lowest energy minimum (Chart 1, Figure 15 and Table 1). According to the relative free energies in solution of the whole set of **DOEC** stereoisomers, an 81:19 population ratio of *trans*-$^{5}C_{8}$ to *cis*-$^{8}C_{5}$ stereosiomers in water solution could be estimated, which also agrees fairly well with the experimental observations.[3]

The most stable structure of compound **3a** shows a *trans* ring fusion (i.e. inversion of nitrogen configuration) and a chair-envelope ($^{8}C_5$-E_{8a}) conformation for the 6- and 5-membered rings (Chart 1). In agreement with the NMR data, the *trans* ring fusion and the chair conformation for the 6-membered ring are maintained in all structures detected up to about 7 kcal mol^{-1}, although alternative envelope conformations for the 5-membered ring appear at the higher energies. Similarly, the most stable stereoisomer of compound **3b** is *trans*-$^{8}C_5$-E_{8a}. However, a *cis*-$^{8}C_5$-E_4 stereoisomer with almost the same free energy and a *cis*-$^{5}C_8$-E_{8a} conformer at ~1.5 kcal mol^{-1} are also detected (Chart 1, Table 1). Taking into account all the structures detected up to about 6.0 kcal mol^{-1} above the lowest energy minimum, a 74:26 *trans*-*cis* population ratio could be estimated for **3b** in water solution (Figure 13), which agrees with the NMR results. Moreover, the lowest energy minimum detected for compound **3c** shows a *cis*-$^{5}C_8$-E_{8a} stereochemistry that coexists with a *trans*-$^{5}C_8$-^{3}E appearing at about 0.4 kcal mol^{-1} (Chart 1, Table 1), which also agrees with the NMR results. Both structures are stabilized by intramolecular hydrogen-bonds between the hydroxymethyl and one of the hydroxyl groups (Chart 1). The estimated *trans*-*cis* population ratio is in this case 57:43 (Figure 15). Finally, in the indolizidine series, compounds **3d** and **3e** show *trans*-$^{5}C_8$-^{8a}E structures as the most stable ones, and all the stereoisomers detected up to about 6.0 kcal mol^{-1} maintain the *trans* ring fusion and the $^{5}C_8$ chair, consistent with the NMR data.

In the quinolizidine series, compounds **4a** and **4b** show the lowest energy minima with *trans*-$^{9}C_6$-$^{1}C_4$ geometry stabilized by intramolecular hydrogen bonds between the 4-hydroxymethyl and the 3-hydroxyl groups (Chart 1). This *trans*-$^{9}C_6$-$^{1}C_4$ arrangement is maintained in all structures detected up to about 3 kcal mol^{-1} (Figure 15). Similarly, compounds **4d** and **4f** show a *trans*-$^{6}C_9$-$^{4}C_1$ disposition for their global energy minima,

and this type of arrangement is also common to all their minima detected up to 3.0 kcal mol^{-1} (Figure 15). On the other hand, compounds **4c** and **4e** show lowest energy minima with *trans*-$^{9}C_{6}$-$^{1}C_{4}$ and *trans*-$^{6}C_{9}$-$^{4}C_{1}$ geometry, respectively. However, both of them yielded *cis* stereoisomers that contribute at higher energies, resulting on estimated *trans*-*cis* population ratios of 52:48 for **4c** and 96:4 for **4e** (Figure 15).

Chart S1. Representative minimum energy structures determined for compounds **3a-e** and **4a-f**, 1-deoxycastanospermine (**DOC**) and 1-deoxy-8a-*epi*-castanospermine (**DOEC**). Intramolecular hydrogen bonds are shown with dotted lines. Each stereoisomer is designated as *cis* or *trans*, considering the disposition of the nitrogen electron pair relative to the hydrogen on the adjacent bridge carbon atom, and with the conformational nomenclature of the two rings (*C*: chair; *E*: envelope) according to IUPAC-IUB Commission on Biochemical Nomenclature (Pure & Appl. Chem. **1981**, *53*, 1901-1905). Ring fusion bond dihedral values ($\theta^{\text{a-b-c-d}}$, degrees) are shown. See Table 1 for full energy details.

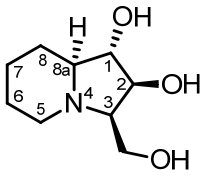 **3a** $\theta^{3\text{-}4\text{-}8a\text{-}1}$, $\theta^{5\text{-}4\text{-}8a\text{-}1}$	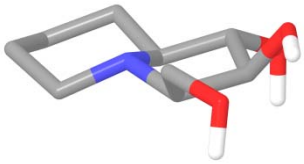 ***trans*-$^{8}C_{5}$-E_{8a}** –43.1 , –170.9		
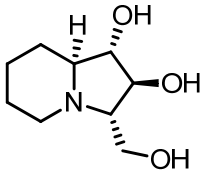 **3b** $\theta^{3\text{-}4\text{-}8a\text{-}1}$, $\theta^{5\text{-}4\text{-}8a\text{-}1}$	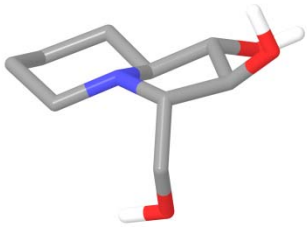 ***trans*-$^{8}C_{5}$-E_{8a}** –39.9 , –178.6	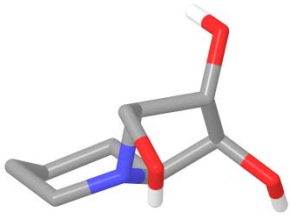 ***cis*-$^{8}C_{5}$-E_{4}** 38.3 , 169.9	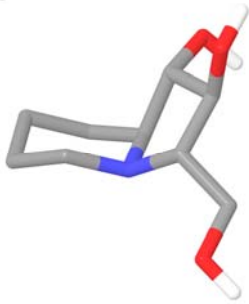 ***cis*-$^{5}C_{8}$-E_{8a}** –37.2 , 85.4
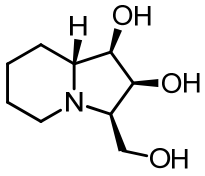 **3c** $\theta^{3\text{-}4\text{-}8a\text{-}1}$, $\theta^{5\text{-}4\text{-}8a\text{-}1}$	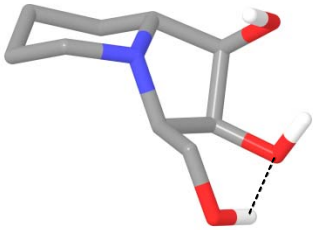 ***cis*-$^{5}C_{8}$-E_{8a}** –38.6 , –171.1	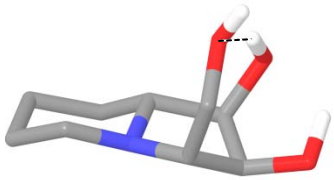 ***trans*-$^{5}C_{8}$-^{3}E** 27.9 , 169.1	
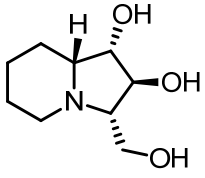 **3d** $\theta^{3\text{-}4\text{-}8a\text{-}1}$, $\theta^{5\text{-}4\text{-}8a\text{-}1}$	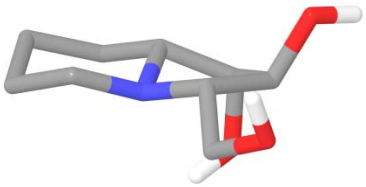 ***trans*-$^{5}C_{8}$-^{8a}E** 49.4 , 177.9		

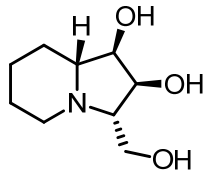 **3e** $\theta^{3\text{-}4\text{-}8a\text{-}1}$, $\theta^{5\text{-}4\text{-}8a\text{-}1}$	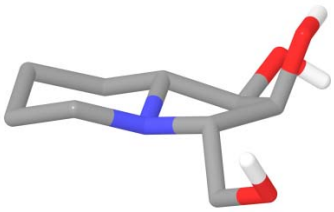 ***trans*-$^{5}C_{8}$-^{8a}E** 44.3 , 174.4		
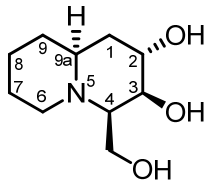 **4a** $\theta^{4\text{-}5\text{-}9a\text{-}1}$, $\theta^{6\text{-}5\text{-}9a\text{-}1}$	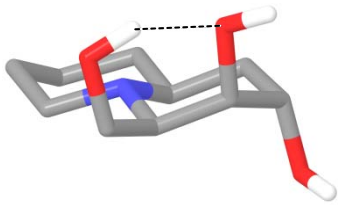 ***trans*-$^{9}C_{6}$-$^{1}C_{4}$** –59.9 , 175.4		
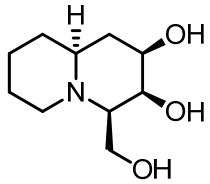 **4b** $\theta^{4\text{-}5\text{-}9a\text{-}1}$, $\theta^{6\text{-}5\text{-}9a\text{-}1}$	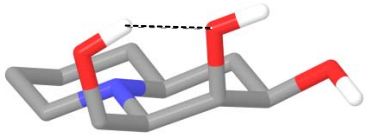 ***trans*-$^{9}C_{6}$-$^{1}C_{4}$** –57.4 , 178.4		
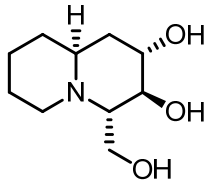 **4c** $\theta^{4\text{-}5\text{-}9a\text{-}1}$, $\theta^{6\text{-}5\text{-}9a\text{-}1}$	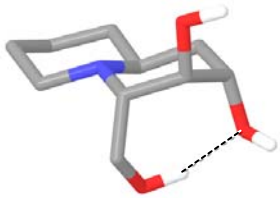 ***trans*-$^{9}C_{6}$-$^{1}C_{4}$** –52.7 , 177.0	 ***cis*-$^{9}C_{6}$-$^{4}C_{1}$** 56.4 , –172.9	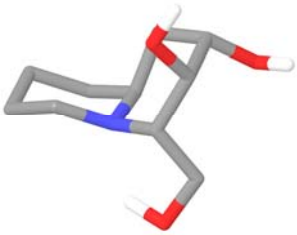 ***cis*-$^{6}C_{9}$-$^{1}C_{4}$** –55.7, 77.5
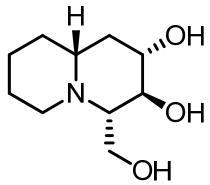 **4d** $\theta^{4\text{-}5\text{-}9a\text{-}1}$, $\theta^{6\text{-}5\text{-}9a\text{-}1}$	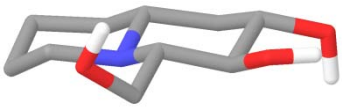 ***trans*-$^{6}C_{9}$-$^{4}C_{1}$** 56.4 , –177.2		
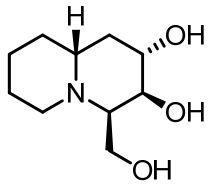 **4e** $\theta^{4\text{-}5\text{-}9a\text{-}1}$, $\theta^{6\text{-}5\text{-}9a\text{-}1}$	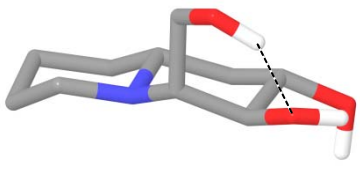 ***trans*-$^{6}C_{9}$-$^{4}C_{1}$** 56.4 , –173.4	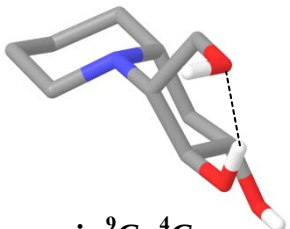 ***cis*-$^{9}C_{6}$-$^{4}C_{1}$** 54.8 , -75.7	

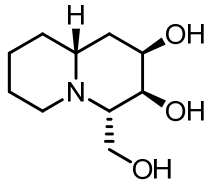		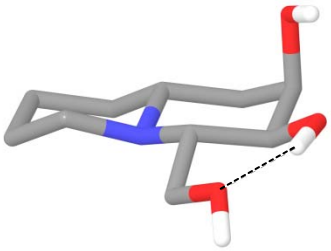
4f $\theta^{4\text{-}5\text{-}9a\text{-}1}$, $\theta^{6\text{-}5\text{-}9a\text{-}1}$		***trans*-$^{6}C_{9}$-$^{4}C_{1}$** 48.5 , 174.6
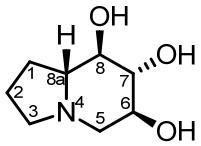		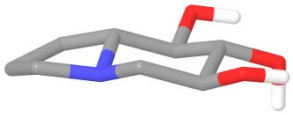
DOC* $\theta^{5\text{-}4\text{-}8a\text{-}8}$, $\theta^{3\text{-}4\text{-}8a\text{-}8}$		***trans*-^{4}E-$^{8}C_{5}$** 64.1 , –166.3
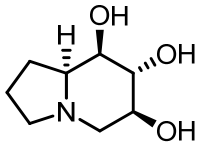	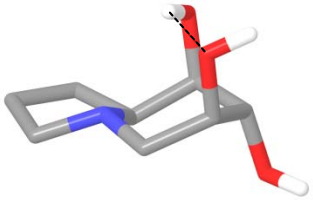	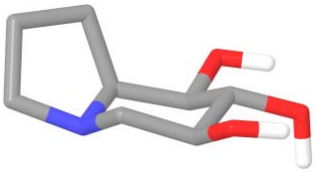
DOEC* $\theta^{5\text{-}4\text{-}8a\text{-}8}$, $\theta^{3\text{-}4\text{-}8a\text{-}8}$	***trans*-E_4-$^{5}C_{8}$** –65.1 , 166.8	***cis*- E_4-$^{8}C_{5}$** 53.3 , 173.6

* Numbering of fused ring system according to Patil et al.[3]

Table S3. Gas phase energy (E^{gp}, hartrees), zero point energy (ZPE, kcal mol^{-1}), enthalpic (ΔH, kcal mol^{-1}) and entropic (ΔS, cal mol^{-1}) corrections at 298.15 K, solvation energy (E^{sol}, kcal mol^{-1}) and relative Gibbs free energies in water solution (ΔG^{wat}, kcal mol^{-1}), determined through density functional theory calculations at B3LYP/cc-pVTZ(-f) level, for the representative minimum energy structures of compounds **3a-e**, **4a-f**, 1-deoxycastanospermine (**DOC**) and 1-deoxy-8a-*epi*-castanospermine (**DOEC**) shown in Chart 1.

Compound and conformation	E^{gp}	ZPE	ΔH	ΔS	E^{sol}	ΔG^{wat}
3a ***trans*-$^{8}C_5$-E_{8a}**	-633.812764	170.94	8.08	105.48	-18.49	0.00
3b ***trans*-$^{8}C_5$-E_{8a}**	-633.809017	170.91	8.16	106.55	-18.02	0.00
***cis*-$^{8}C_5$-E_4**	-633.806935	170.89	8.12	106.16	-19.32	0.07
***cis*-$^{5}C_8$-E_{8a}**	-633.801656	170.80	8.15	106.44	-21.10	1.45
3c ***cis*-$^{5}C_8$-E_{8a}**	-633.815424	171.08	8.00	104.61	-14.51	0.00
***trans*-$^{5}C_8$-^{3}E**	-633.815691	171.20	7.93	103.85	-14.24	0.38
3d ***trans*-$^{5}C_8$-^{8a}E**	-633.812316	170.86	8.16	106.38	-18.15	0.00
3e ***trans*-$^{5}C_8$-^{8a}E**	-633.812863	170.99	8.10	105.98	-18.82	0.00
4a ***trans*-$^{9}C_6$-$^{1}C_4$**	-673.138649	189.36	8.72	109.87	-19.02	0.00
4b ***trans*-$^{9}C_6$-$^{1}C_4$**	-673.143543	189.47	8.70	109.55	-17.01	0.00
4c ***trans*-$^{9}C_6$-$^{1}C_4$**	-673.137109	189.50	8.67	109.30	-19.10	0.00
***cis*-$^{9}C_6$-$^{4}C_1$**	-673.140209	189.40	8.79	110.45	-16.49	0.35
***cis*-$^{6}C_9$-$^{1}C_4$**	-673.136600	189.34	8.79	110.67	-15.90	3.08
4d ***trans*-$^{6}C_9$-$^{4}C_1$**	-673.142973	189.40	8.82	110.87	-17.16	0.00
4e ***trans*-$^{6}C_9$-$^{4}C_1$**	-673.143307	189.60	8.71	109.82	-16.62	0.00
***cis*-$^{9}C_6$-$^{4}C_1$**	-673.140140	189.55	8.70	109.72	-16.68	1.90
4f ***trans*-$^{6}C_9$-$^{4}C_1$**	-673.145062	189.68	8.68	109.55	-15.70	0.00
DOC ***trans*-^{4}E-$^{8}C_5$**	-594.492000	152.54	7.29	99.11	-17.05	0.00
DOEC ***trans*-E_4-$^{5}C_8$**	-594.488048	152.46	7.28	99.00	-16.62	0.00
***cis*-E_4-$^{8}C_5$**	-594.483351	152.55	7.29	99.14	-18.59	1.04

Figure 15. Distribution of relative free energies in water (ΔG^{wat}, kcal mol^{-1}) *vs* ring fusion bond dihedrals ($\theta^{a\text{-}b\text{-}c\text{-}d}$, degrees, see Chart S1 for definition of dihedral atoms for each compound), for minima determined for compounds **3a-e**, **4a-f**, 1-deoxycastanospermine (**DOC**) and 1-deoxy-8a-*epi*-castanospermine (**DOEC**). Number of minima detected for each compound (N) is shown.

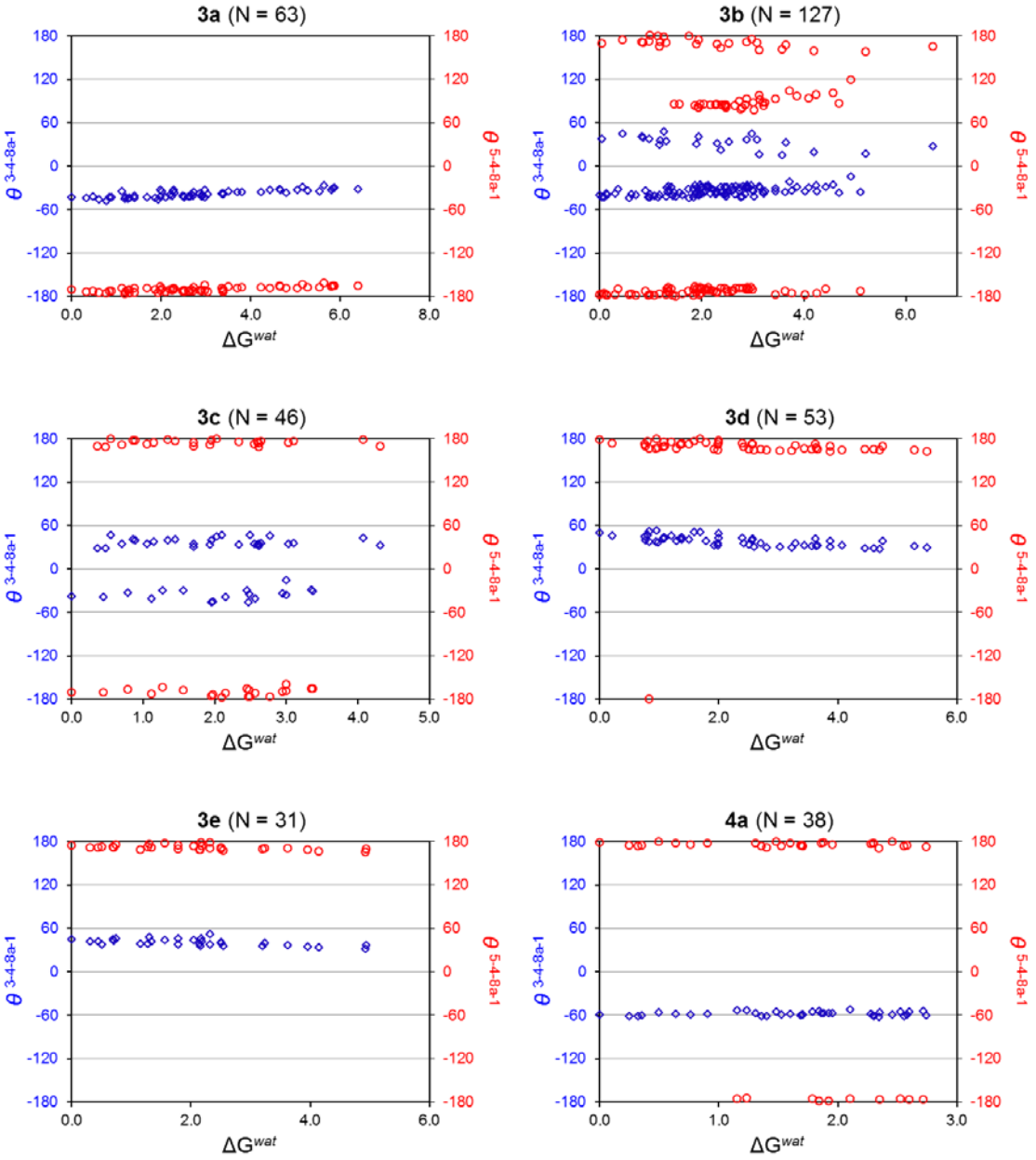

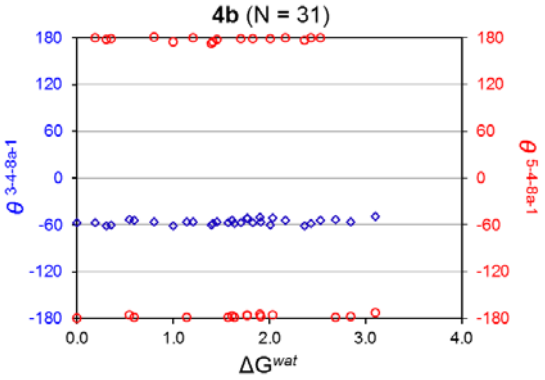

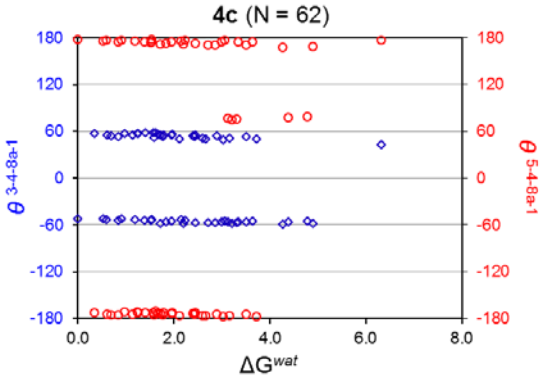

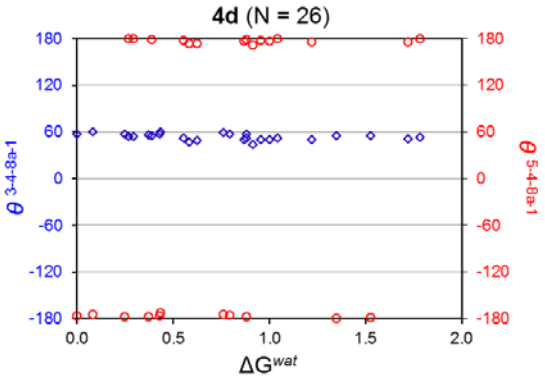

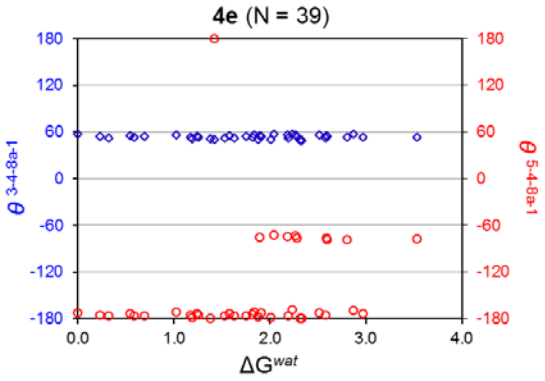

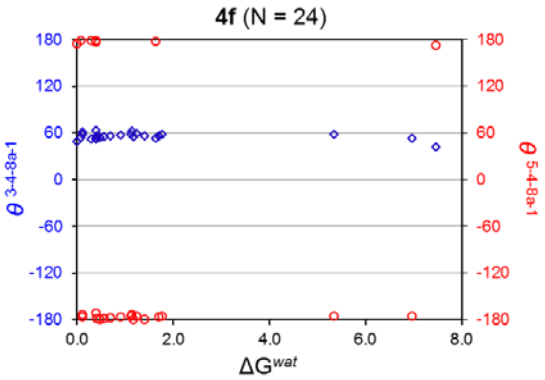

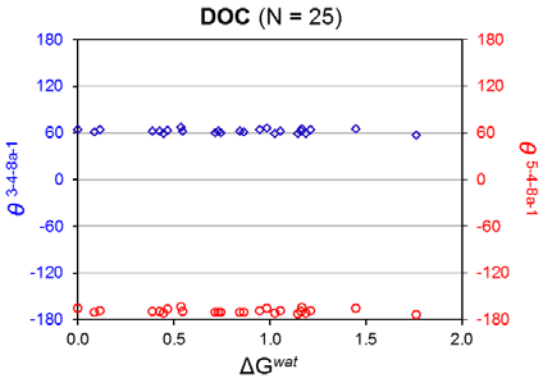

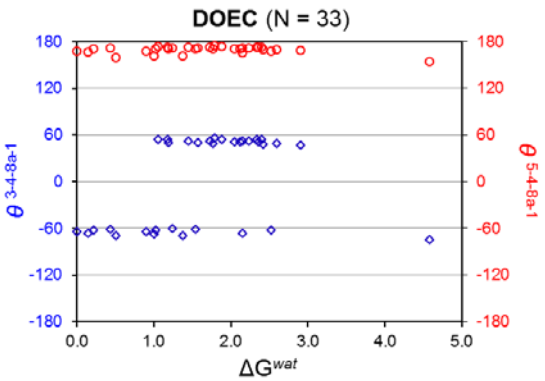

References

1. A. Dahlqvist, *Anal. Biochem.*, 1964, **7**, 18-25.
2. M. M. Bradford, *Anal. Biochem.*, 1976, **72**, 248-254.
3. N. T. Patil, J. N. Tilekar and D. D. Dhavale, *Tetrahedron Lett.*, 2001, **42**, 747-749; N. T. Patil, J. N. Tilekar and D. D. Dhavale, *J. Org. Chem.*, 2001, **66**, 1065-1074.
4. Cis/trans ring fusion can arise from inversion of the configuration of the bridgehead nitrogen, which normally is associated with a confomational change on one or both rings of the indolizidine or quinolizidine.